canonical ADAMs (Supplementary Figure 1). Comparison of the recently solved ADAM10 D/C-domain partial structure ($ADAM10_{D+C}$) (Janes *et al*, 2005) and that of VAP1 reveals that the atypical ADAM10 shares the continuous D_a/C_w structure and the C_h-domain scaffold with VAP1; however, it has an disordered D_s-domain and an alternate HVR structure and a different orientation between C_w- and C_h-domains (Figure 6). The locations of four of the five disulfide bridges within the C_h-domain are conserved between VAP1 and ADAM10 (Figure 6B and C) and thus, they enabled us to align the two sequences (Figure 6E). Based on this alignment, we completed entire alignments (Supplementary Figure 1) including 38 sequences of mammalian ADAMs and *Schizosaccharomyces pombe* Mde10 (Nakamura *et al*, 2004), presumably the founding member of the ADAM family in evolutionary terms. The $ADAM10_{D+C}$ structure lacks the eight residues (583–590 in ADAM10) that may form a flexible loop. However, VAP1 (Figure 6E) and the canonical ADAMs except for ADAM8 (Supplementary Figure 1) have extra 16 residues in this segment that, in part, forms a variable loop, flanked by the adjacent cysteinyl residues (Cys539 and Cys549 in VAP1) and protrudes from the main body of the C-domain (Figures 4A and 6B). The variable loop has highest temperature factor in the molecule and resembles to the disintegrin-loop, thus can be an additional protein-binding interface. The six VAP1 monomer molecules represent almost the same C_w/C_h domain orientation (data not shown), however that is distinct from that of ADAM10 (Figure 5A). Thus, the possibility whether different ADAMs have distinct C_w/C_h domain orientation remains to be established. Janes *et al* (2005) have shown that the three glutamate residues outside of HVR are essential for ADAM10-mediated ephrin proteolysis in *trans*, however, roles of the ADAM10 HVR has not been examined. An extensive molecular surface of the elongated arm structure (12 000 Å^2 for the VAP1 D/C-domains) might reveal additional protein–protein interaction interfaces other than the HVR. Multiple charged residues in the D-domain are essential for ADAM28 binding to $\alpha4\beta1$ (Bridges *et al*, 2003) and the RX_6DLPEF motif has been proposed for integrin $\alpha9\beta1$ binding (Eto *et al*, 2002). However, the D-domain portion of the C-shaped scaffold is away from the catalytic site; thus, those additional sites might not directly serve as target recognition interfaces for catalysis.

Uniquely among cell-surface proteins, ADAMs display both proteolytic and adhesive activities. The VAP1 structure reveals that these functions are spatially allocated to the ends of the unique C-shaped scaffold and face each other. This spatial allocation of the functional sites provide us insights

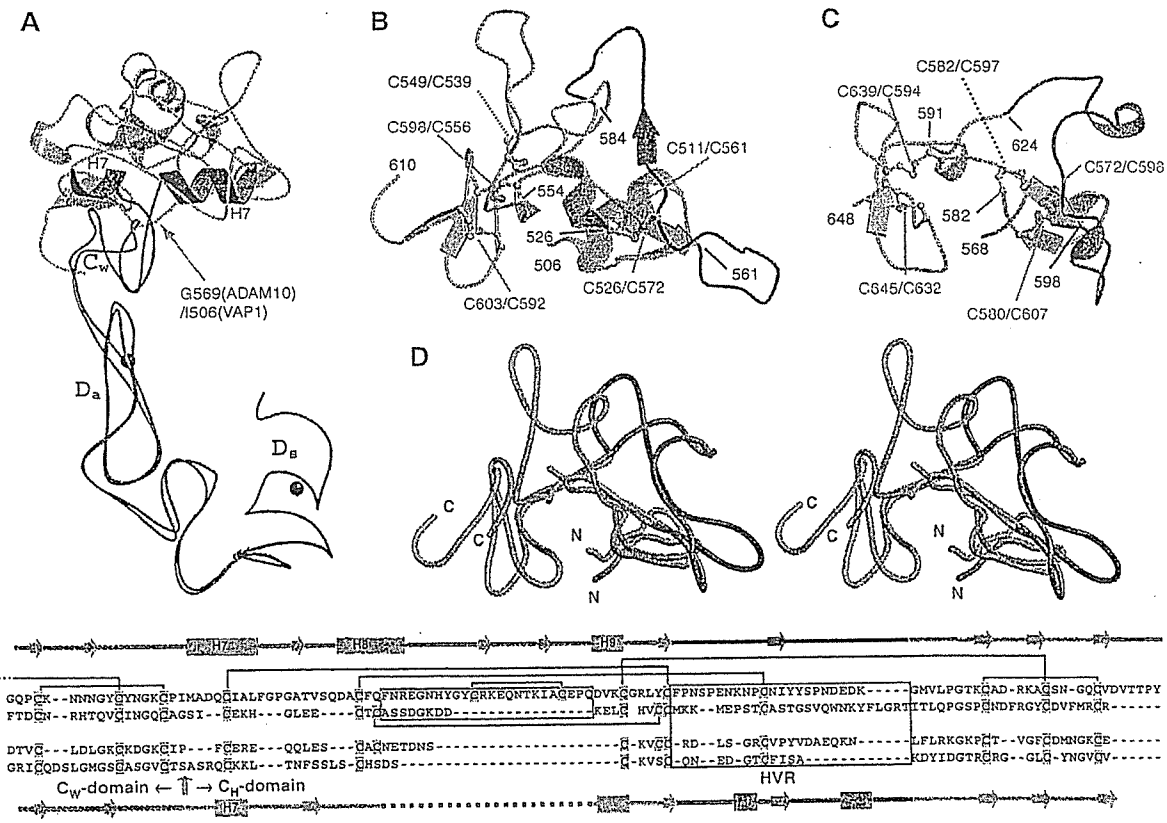

Figure 6 Comparison of the VAP1 and ADAM10 D/C domains. (A) Superimposition of the D_a-domains of ADAM10 and VAP1. The $D_s/D_a/C_w$-domains and the H7 helix of VAP1 and those of ADAM10 are shown in blue and red, respectively. The C_h-domains of VAP1 and ADAM10 are shown in cyan and pink, respectively. The arrow indicates the pivotal point between the C_w- and C_h-domains. Bound Ca^{2+} ions in VAP1 are shown as black spheres. (B) Ribbon representation of the C_h-domain of VAP1. The HVR is shown in blue. The common scaffold between the VAP1 and ADAM10 C_h-domains are shown in cyan and the segment lacking in ADAM10 is shown in light green. Disulfide bridges are indicated. (C) Ribbon representation of the C_h-domain of ADAM10. The HVR is shown in red. Disulfide brides are indicated. (D) Superimposition of the C_h-domains of VAP1 and ADAM10 *in stereo* with the colors as in (B, C). The N- and C-termini of the C_h-domains are indicated. (E) Structure-based alignments of VAP1, bovine ADAM10 (cADAM10), human ADAM17 (hADAM17) and *S. pombe* Mde10 (Mde10) C_w/C_h-domains. Secondary structures and the disulfide bridges are represented schematically. The HVR sequences and the missing segment in the ADAM10 structure are boxed in blue and green, respectively.

topologies and should be grouped into a common family, the 'metzincins'. *FEBS Lett* 331: 134–140

Bridges LC, Hanson KR, Tani PH, Mather T, Bowditch RD (2003) Integrin alpha4beta1-dependent adhesion to ADAM 28 (MDC-L) requires an extended surface of the disintegrin domain. *Biochemistry* 42: 3734–3741

Brunger AT, Adams PD, Clore GM, DeLano WL, Gros P, Grosse-Kunstleve RW, Jiang JS, Kuszewski J, Nilges M, Pannu NS, Read RJ, Rice LM, Simonson T, Warren GL (1998) Crystallography & NMR system: a new software suite for macromolecular structure determination. *Acta Crystallogr D* 54 (Part 5): 905–921

Calvete JJ, Marcinkiewicz C, Monleon D, Esteve V, Celda B, Juarez P, Sanz L (2005) Snake venom disintegrins: evolution of structure and function. *Toxicon* 45: 1063–1074

CCP4 (1994) The CCP4 suite: programs for protein crystallography. *Acta Crystallogr D* 50: 760–763

Duffy MJ, Lynn DJ, Lloyd AT, O'Shea CM (2003) The ADAMs family of proteins: from basic studies to potential clinical applications. *Thromb Haemost* 89: 622–631

Eto K, Huet C, Tarui T, Kupriyanov S, Liu HZ, Puzon-McLaughlin W, Zhang XP, Sheppard D, Engvall E, Takada Y (2002) Functional classification of ADAMs based on a conserved motif for binding to integrin alpha 9beta 1: implications for sperm-egg binding and other cell interactions. *J Biol Chem* 277: 17804–17810

Evans JP (2001) Fertilin beta and other ADAMs as integrin ligands: insights into cell adhesion and fertilization. *BioEssays* 23: 628–639

Fox JW, Serrano SM (2005) Structural considerations of the snake venom metalloproteinases, key members of the M12 reprolysin family of metalloproteinases. *Toxicon* 45: 969–985

Fujii Y, Okuda D, Fujimoto Z, Horii K, Morita T, Mizuno H (2003) Crystal structure of trimestatin, a disintegrin containing a cell adhesion recognition motif RGD. *J Mol Biol* 332: 1115–1122

Gaultier A, Cousin H, Darribere T, Alfandari D (2002) ADAM13 disintegrin and cysteine-rich domains bind to the second heparin-binding domain of fibronectin. *J Biol Chem* 277: 23336–23344

Huang TF, Holt JC, Lukasiewicz H, Niewiarowski S (1987) Trigramin. A low molecular weight peptide inhibiting fibrinogen interaction with platelet receptors expressed on glycoprotein lib-IIIa complex. *J Biol Chem* 262: 16157–16163

Iba K, Albrechtsen R, Gilpin B, Frohlich C, Loechel F, Zolkiewska A, Ishiguro K, Kojima T, Liu W, Langford JK, Sanderson RD, Brakebusch C, Fassler R, Wewer UM (2000) The cysteine-rich domain of human ADAM 12 supports cell adhesion through syndecans and triggers signaling events that lead to beta1 integrin-dependent cell spreading. *J Cell Biol* 149: 1143–1156

Janes PW, Saha N, Barton WA, Kolev MV, Wimmer-Kleikamp SH, Nievergall E, Blobel CP, Himanen JP, Lackmann M, Nikolov DB (2005) Adam meets Eph: an ADAM substrate recognition module acts as a molecular SWITCH for Ephrin cleavage *in trans*. *Cell* 123: 291–304

Jia LG, Shimokawa K, Bjarnason JB, Fox JW (1996) Snake venom metalloproteinases: structure, function and relationship to the ADAMs family of proteins. *Toxicon* 34: 1269–1276

Jia LG, Wang XM, Shannon JD, Bjarnason JB, Fox JW (2000) Inhibition of platelet aggregation by the recombinant cysteine-rich domain of the hemorrhagic snake venom metalloproteinase, atrolysin A. *Arch Biochem Biophys* 373: 281–286

Kamiguti AS, Gallagher P, Marcinkiewicz C, Theakston RD, Zuzel M, Fox JW (2003) Identification of sites in the cysteine-rich domain of the class P-III snake venom metalloproteinases responsible for inhibition of platelet function. *FEBS Lett* 549: 129–134

Maskos K, Fernandez-Catalan C, Huber R, Bourenkov GP, Bartunik H, Ellestad GA, Reddy P, Wolfson MF, Rauch CT, Castner BJ, Davis R, Clarke HR, Petersen M, Fitzner JN, Cerretti DP, March CJ, Paxton RJ, Black RA, Bode W (1998) Crystal structure of the catalytic domain of human tumor necrosis factor-alpha-converting enzyme. *Proc Natl Acad Sci USA* 95: 3408–3412

Masuda S, Hayashi H, Araki S (1998) Two vascular apoptosis-inducing proteins from snake venom are members of the metalloprotease/disintegrin family. *Eur J Biochem* 253: 36–41

Masuda S, Ohta T, Kaji K, Fox JW, Hayashi H, Araki S (2000) cDNA cloning and characterization of vascular apoptosis-inducing protein 1. *Biochem Biophys Res Commun* 278: 197–204

Moss ML, Bartsch JW (2004) Therapeutic benefits from targeting of ADAM family members. *Biochemistry* 43: 7227–7235

Moss ML, Jin SL, Milla ME, Bickett DM, Burkhart W, Carter HL, Chen WJ, Clay WC, Didsbury JR, Hassler D, Hoffman CR, Kost TA, Lambert MH, Leesnitzer MA, McCauley P, McGeehan G, Mitchell J, Moyer M, Pahel G, Rocque W, Overton LK, Schoenen F, Seaton T, Su JL, Warner J, Willard D, Becherer JD (1997) Cloning of a disintegrin metalloproteinase that processes precursor tumour-necrosis factor-alpha. *Nature* 385: 733–736

Myles DG, Kimmel LH, Blobel CP, White JM, Primakoff P (1994) Identification of a binding site in the disintegrin domain of fertilin required for sperm-egg fusion. *Proc Natl Acad Sci USA* 91: 4195–4198

Nakamura T, Abe H, Hirata A, Shimoda C (2004) ADAM family protein Mde10 is essential for development of spore envelopes in the fission yeast *Schizosaccharomyces pombe*. *Eukaryot Cell* 3: 27–39

Orth P, Reichert P, Wang W, Prosise WW, Yarosh-Tomaine T, Hammond G, Ingram RN, Xiao L, Mirza UA, Zou J, Strickland C, Taremi SS, Le HV, Madison V (2004) Crystal structure of the catalytic domain of human ADAM33. *J Mol Biol* 335: 129–137

Pan D, Rubin GM (1997) Kuzbanian controls proteolytic processing of Notch and mediates lateral inhibition during *Drosophila* and vertebrate neurogenesis. *Cell* 90: 271–280

Perrakis A, Morris R, Lamzin VS (1999) Automated protein model building combined with iterative structure refinement. *Nat Struct Biol* 6: 458–463

Primakoff P, Hyatt H, Tredick-Kline J (1987) Identification and purification of a sperm surface protein with a potential role in sperm-egg membrane fusion. *J Cell Biol* 104: 141–149

Qi H, Rand MD, Wu X, Sestan N, Wang W, Rakic P, Xu T, Artavanis-Tsakonas S (1999) Processing of the notch ligand delta by the metalloprotease Kuzbanian. *Science* 283: 91–94

Reddy P, Slack JL, Davis R, Cerretti DP, Kozlosky CJ, Blanton RA, Shows D, Peschon JJ, Black RA (2000) Functional analysis of the domain structure of tumor necrosis factor-alpha converting enzyme. *J Biol Chem* 275: 14608–14614

Rooke J, Pan D, Xu T, Rubin GM (1996) KUZ, a conserved metalloprotease-disintegrin protein with two roles in *Drosophila* neurogenesis. *Science* 273: 1227–1231

Seals DF, Courtneidge SA (2003) The ADAMs family of metalloproteases: multidomain proteins with multiple functions. *Genes Dev* 17: 7–30

Serrano SM, Jia LG, Wang D, Shannon JD, Fox JW (2005) Function of the cysteine-rich domain of the haemorrhagic metalloproteinase atrolysin A: targeting adhesion proteins collagen I and von Willebrand factor. *Biochem J* 391: 69–76

Smith KM, Gaultier A, Cousin H, Alfandari D, White JM, DeSimone DW (2002) The cysteine-rich domain regulates ADAM protease function *in vivo*. *J Cell Biol* 159: 893–902

Van Eerdewegh P, Little RD, Dupuis J, Del Mastro RG, Falls K, Simon J, Torrey D, Pandit S, McKenny J, Braunschweiger K, Walsh A, Liu Z, Hayward B, Folz C, Manning SP, Bawa A, Saracino L, Thackston M, Benchekroun Y, Capparell N, Wang M, Adair R, Feng Y, Dubois J, FitzGerald MG, Huang H, Gibson R, Allen KM, Pedan A, Danzig MR, Umland SP, Egan RW, Cuss FM, Rorke S, Clough JB, Holloway JW, Holgate ST, Keith TP (2002) Association of the ADAM33 gene with asthma and bronchial hyperresponsiveness. *Nature* 418: 426–430

White JM (2003) ADAMs: modulators of cell–cell and cell–matrix interactions. *Curr Opin Cell Biol* 15: 598–606

Yagami-Hiromasa T, Sato T, Kurisaki T, Kamijo K, Nabeshima Y, Fujisawa-Sehara A (1995) A metalloprotease-disintegrin participating in myoblast fusion. *Nature* 377: 652–656

Zhu X, Teng M, Niu L (1999) Structure of acutolysin-C, a haemorrhagic toxin from the venom of Agkistrodon acutus, providing further evidence for the mechanism of the pH-dependent proteolytic reaction of zinc metalloproteinases. *Acta Crystallogr D* 55: 1834–1841

Zolkiewska A (1999) Disintegrin-like/cysteine-rich region of ADAM 12 is an active cell adhesion domain. *Exp Cell Res* 252: 423–431

into the molecular mechanism of ADAMs' target recognition, which ADAMs shed which key substrates in specific biological events. Since ADAMs are potential therapeutic targets, the distinct surface feature created by the HVR of the individual ADAMs might also provide insights into the future design of drugs with higher specificity for each member of ADAMs. We suggest that the HVR, not the disintegrin domain, should be the focus of searches for physiological targets of ADAMs.

Materials and methods

Protein preparation and crystallization

The details of the preparation, crystallization and preliminary X-ray analysis of VAP1 will be described elsewhere (T Igarashi *et al*, in preparation). VAP1 was isolated from the crude snake *Crotalus atrox* venom (Sigma-Aldrich, USA) and subjected to sitting- or hanging-drop vapor diffusion crystallization. Two distinct crystal forms ($P2_12_12_1$ and $P4_12_12$) were obtained with the reservoir solution containing 15% polyethyleneglycol 8000 and 100 mM sodium cacodylate at pH 6.5, with (orthorhombic form) or without (tetragonal form) 20 mM cobaltous chloride hexahydrate. GM6001-bound crystals were prepared by adding GM6001 (CALBIOCHEM) to the drop with the orthorhombic crystal at a final concentration qof 0.33 mM (twice the protein concentration) followed by a 12-h incubation. Crystals were flash-frozen under the nitrogen flow at 90 K.

Diffraction data collection

All the diffraction data were collected at SPring-8 beamlines using either ADSC quantum 310R CCD (for the inhibitor-bound crystal at the beamline BL41XU with $\lambda = 1$ Å), Rigaku *R*-axis V imaging plate (for orthorhombic native crystal at the beamline BL45PX with $\lambda = 1$ Å) or Jupitor CCD (for the tetragonal crystal at the beamline BL45PX with $\lambda = 0.98$ Å) detectors at 90 K. The images were reduced using HKL2000. Both orthorhombic and tetragonal native data sets were collected to 2.5-Å resolution and inhibitor-bound crystal data sets were collected to 3.0 Å resolution (Table I).

Structural analysis

All structures were solved by the molecular replacement method by MOLREP in the CCP4 suite (CCP4, 1994) by using acutolysin-C (1QUA) (Zhu *et al*, 1999) as a starting model. Initially, the MR solution obtained from the orthorhombic crystal data set, assumed two M-domains in the asymmetric units. After manual rebuilding by TURBO-FRODO, the model was subjected to tortional molecular dynamic refinements with restrained NCS averaging of the M-domains using CNS (Brunger *et al*, 1998) and iterative refinements and manual rebuilding of the model improved the electron-density map and enabled us to extend the model. First, we found the electron densities associated with the pieces of helical segments of the molecules and modelled them as poly-alanine chains. After cycles of refinements, we assigned those segments as the parts of helices H7 and H8, where the secondary structures are predicted to be helices, judging from the electron densities associated with the side chains. At this stage, four tyrosine residues, Tyr575 and Try576 within the central β strands of the HVRs were clearly defined, and we noticed that there was another NCS-axis between the C-domains. After iterative rounds of refinements with restrained NCS averaging of the C-domains and manual model building, we completed modelling of the C-domains. From this stage onward, no NCS averaging was included in the refinements. Next, we modelled the D-domains with the help of automated chain tracing using the program ARP/wARP (Perrakis *et al*, 1999) and with the structural model of trimestatin (1J2L) as a guide. After completely modelling the polypeptide chains, we noticed that isolated lobes of high electron densities surrounded by oxygen atoms occurred both in the D_s- and D_a-domains. For these sites, calcium ions fit optimally to the electron density with a refined occupancy of 100% and reasonably low *B*-values, thus, we included calcium ions in the model. We also assigned a cobalt ion, which was supplemented in the crystallization buffer for the orthorhombic crystal form, located between the M- and D_s-domains in the A molecule. The part of the carbohydrate chain linked to residue Asn218 (two *N*-acetylglocosamine (NAG) moieties) was modelled. Then, water molecules were assigned. The *VAP1* cDNA encodes a protein with 610 amino-acid residues; however, the N-terminus is processed by post-translational modification (Masuda *et al*, 1998, 2000). Here, protein sequencing of the de-blocked VAP1 molecule clarified that the Glu184 side chain was modified into a pyro-form. The electron densities associated with almost the entire molecule except for the first pyroglutamic acid were defined in either monomer within the orthorhombic crystal. In the final model, 86.1% of the residues lay in the most favorable region, 13.3% in the additionally allowed region and 0.7% in the generously allowed region of the Ramachandran plot. The tetragonal crystal and inhibitor-bound crystal were solved by MR with the domains of the refined orthorhombic apo-form as a starting model. In the final model, 83.6% (80.6%) of the residues lay in the most favorable region, 15.7% (18.9%) in the additionally allowed region and 0.7% (0.5%) in the generously allowed region for tetragonal (inhibitor-bound) crystals in the Ramachandran plot. In either crystal form, the asymmetric unit contained one dimer molecule. All six monomers had almost identical structures. Refinement statistics are shown in Table I.

PDB accession codes

Atomic coordinates and structure factors have been deposited in the Protein Data Bank under accession codes 2ERO, 2ERP and 2ERQ for the orthorhombic native, GM6001-bound form and tetragonal-form, respectively.

Supplementary data

Supplementary data are available at *The EMBO Journal* Online.

Acknowledgements

We thank Yuko Oishi and staff in SPring-8 beamlines for assistance with data acquisition and Junichi Takagi for discussions and critical reading of the manuscript. This work was partly supported by Grant nano-001 for Research on Advanced Medical Technology from the Ministry of Health, Labor, and Welfare of Japan, and by grants from the Takeda Science Foundation, from the Kao Foundation for Arts and Science and from Senri Life Science Foundation. The authors declare no competing financial interests.

References

Almeida EA, Huovila AP, Sutherland AE, Stephens LE, Calarco PG, Shaw LM, Mercurio AM, Sonnenberg A, Primakoff P, Myles DG, White JM (1995) Mouse egg integrin alpha 6 beta 1 functions as a sperm receptor. *Cell* 81: 1095–1104

Becherer JD, Blobel CP (2003) Biochemical properties and functions of membrane-anchored metalloprotease-disintegrin proteins (ADAMs). *Curr Top Dev Biol* 54: 101–123

Black RA, Rauch CT, Kozlosky CJ, Peschon JJ, Slack JL, Wolfson MF, Castner BJ, Stocking KL, Reddy P, Srinivasan S, Nelson N, Boiani N, Schooley KA, Gerhart M, Davis R, Fitzner JN, Johnson RS, Paxton RJ, March CJ, Cerretti DP (1997) A metalloproteinase disintegrin that releases tumour-necrosis factor-alpha from cells. *Nature* 385: 729–733

Blobel CP (2005) ADAMs: key components in EGFR signalling and development. *Nat Rev Mol Cell Biol* 6: 32–43

Blobel CP, Myles DG, Primakoff P, White JM (1990) Proteolytic processing of a protein involved in sperm-egg fusion correlates with acquisition of fertilization competence. *J Cell Biol* 111: 69–78

Blobel CP, Wolfsberg TG, Turck CW, Myles DG, Primakoff P, White JM (1992) A potential fusion peptide and an integrin ligand domain in a protein active in sperm-egg fusion. *Nature* 356: 248–252

Bode W, Gomis-Ruth FX, Stockler W (1993) Astacins, serralysins, snake venom and matrix metalloproteinases exhibit identical zinc-binding environments (HEXXHXXGXXH and Met-turn) and

Am J Physiol Heart Circ Physiol 291: H1138–H1146, 2006.
First published April 28, 2006; doi:10.1152/ajpheart.00187.2006.

Cardioprotective role of endogenous hydrogen peroxide during ischemia-reperfusion injury in canine coronary microcirculation in vivo

Toyotaka Yada,[1] Hiroaki Shimokawa,[3] Osamu Hiramatsu,[1] Yoshisuke Haruna,[2] Yoshitaka Morita,[2] Naoki Kashihara,[2] Yoshiro Shinozaki,[4] Hidezo Mori,[5] Masami Goto,[1] Yasuo Ogasawara,[1] and Fumihiko Kajiya[1]

[1]*Department of Medical Engineering and Systems Cardiology and* [2]*Division of Nephrology and Rheumatology, Department of Internal Medicine, Kawasaki Medical School, Kurashiki;* [3]*Department of Cardiovascular Medicine, Tohoku University Graduate School of Medicine, Sendai;* [4]*Department of Physiology, Tokai University School of Medicine, Isehara; and* [5]*Department of Cardiac Physiology, National Cardiovascular Center Research Institute, Suita, Japan*

Submitted 22 February 2006; accepted in final form 18 April 2006

Yada, Toyotaka, Hiroaki Shimokawa, Osamu Hiramatsu, Yoshisuke Haruna, Yoshitaka Morita, Naoki Kashihara, Yoshiro Shinozaki, Hidezo Mori, Masami Goto, Yasuo Ogasawara, and Fumihiko Kajiya. Cardioprotective role of endogenous hydrogen peroxide during ischemia-reperfusion injury in canine coronary microcirculation in vivo. *Am J Physiol Heart Circ Physiol* 291: H1138–H1146, 2006. First published April 28, 2006; doi:10.1152/ajpheart.00187.2006.—We have recently demonstrated that endogenous H_2O_2 plays an important role in coronary autoregulation in vivo. However, the role of H_2O_2 during coronary ischemia-reperfusion (I/R) injury remains to be examined. In this study, we examined whether endogenous H_2O_2 also plays a protective role in coronary I/R injury in dogs in vivo. Canine subepicardial small coronary arteries (≥100 μm) and arterioles (<100 μm) were continuously observed by an intravital microscope during coronary I/R (90/60 min) under cyclooxygenase blockade ($n = 50$). Coronary vascular responses to endothelium-dependent vasodilators (ACh) were examined before and after I/R under the following seven conditions: control, nitric oxide (NO) synthase (NOS) inhibitor N^G-monomethyl-L-arginine (L-NMMA), catalase (a decomposer of H_2O_2), 8-sulfophenyltheophylline (8-SPT, an adenosine receptor blocker), L-NMMA + catalase, L-NMMA + tetraethylammonium (TEA, an inhibitor of large-conductance Ca^{2+}-sensitive potassium channels), and L-NMMA + catalase + 8-SPT. Coronary I/R significantly impaired the coronary vasodilatation to ACh in both sized arteries (both $P < 0.01$); L-NMMA reduced the small arterial vasodilatation (both $P < 0.01$), whereas it increased ($P < 0.05$) the ACh-induced coronary arteriolar vasodilatation associated with fluorescent H_2O_2 production after I/R. Catalase increased the small arterial vasodilatation ($P < 0.01$) associated with fluorescent NO production and increased endothelial NOS expression, whereas it decreased the arteriolar response after I/R ($P < 0.01$). L-NMMA + catalase, L-NMMA + TEA, or L-NMMA + catalase + 8-SPT further decreased the coronary vasodilatation in both sized arteries (both, $P < 0.01$). L-NMMA + catalase, L-NMMA + TEA, and L-NMMA + catalase + 8-SPT significantly increased myocardial infarct area compared with the other four groups (control, L-NMMA, catalase, and 8-SPT; all, $P < 0.01$). These results indicate that endogenous H_2O_2, in cooperation with NO, plays an important cardioprotective role in coronary I/R injury in vivo.

endothelium-derived relaxing factor; myocardial infarction; vascular endothelial function

VASCULAR ENDOTHELIAL CELLS play an important role in maintaining vascular homeostasis by synthesizing and releasing endothelium-derived relaxing factors (EDRFs), including prostacyclin (PGI_2), nitric oxide (NO), and endothelium-derived hyperpolarizing factor (EDHF) (6, 9, 26). Endothelial dysfunction is thus characterized by a reduction in the activity of PGI_2, NO, and EDHF, thereby enhancing vasoconstrictor responses mediated by endothelin, serotonin, and thrombin (26). Endothelial injury secondary to myocardial ischemia-reperfusion (I/R) decreases the production and activity of EDRFs in acute myocardial infarction (18).

Among the three different EDRFs, the roles of PGI_2 and NO have been extensively investigated (6, 9, 26). Regarding EDHF, since the first reports on its existence (6, 9), several candidates for EDHF have been proposed, including cytochrome *P*-450 metabolites (2, 4), endothelium-derived K^+ (7), and electrical communications through gap junctions between endothelial cells and vascular smooth muscle cells (29). Matoba et al. (16, 17) have previously identified that endothelium-derived H_2O_2 is a primary EDHF in mesenteric arteries of mice and humans. Morikawa et al. (21) have recently confirmed that endothelial Cu,Zn-SOD plays an important role as an EDHF synthase in mice. We have subsequently confirmed the importance of H_2O_2 in canine coronary microcirculation during coronary autoregulation with reduced coronary perfusion pressure in vivo (35).

However, it remains to be examined whether H_2O_2 also exerts cardioprotective effects during I/R in the coronary microcirculation in vivo, and if so, whether such effects of H_2O_2 compensate the impaired NO-mediated responses due to I/R injury in vivo. In this study, we tested our hypothesis that H_2O_2 plays an important cardioprotective and compensatory role during coronary I/R injury in dogs in vivo.

METHODS

This study conformed to the Guideline on Animal Experiments of Kawasaki Medical School, and approved by an independent review committee from the same institution, and the *Guide for the Care and Use of Laboratory Animals* published by the National Institutes of Health.

Animal preparation. Anesthetized mongrel dogs (15–25 kg in body wt, $n = 50$) of either sex were ventilated with a ventilator (model VS600, IDC, Pittsburgh, PA). Aortic pressure and left ventricular (LV) pressure were continuously monitored with a catheter (SPC-784A, Millar, TX). The blood flow of the left anterior descending coronary artery (LAD) was continuously measured by a transonic flow probe (T206, Transonic Systems, Ithaca, NY).

Address for reprint requests and other correspondence: T. Yada, Dept. of Medical Engineering and Systems Cardiology, Kawasaki Medical School, 577 Matsushima, Kurashiki, Okayama 701-0192, Japan (e-mail: yada@me.kawasaki-m.ac.jp).

The costs of publication of this article were defrayed in part by the payment of page charges. The article must therefore be hereby marked "*advertisement*" in accordance with 18 U.S.C. Section 1734 solely to indicate this fact.

Measurements of coronary diameter by intravital microscope. We continuously monitored coronary vascular responses by an intravital microscope (VMS 1210, Nihon-Kohden, Tokyo) with a needle probe in vivo as previously described (32). We gently placed the needle probe on subepicardial microvessels. When a clear vascular image was obtained, end-diastolic vascular images were taken with 30 pictures/s (32).

Measurements of regional myocardial blood flow. Regional myocardial blood flow was measured by the nonradioactive microsphere (Sekisui Plastic, Tokyo) technique, as previously described (20). Briefly, the microsphere suspension was injected into the left atrium 85 min after the onset of coronary occlusion. Myocardial collateral flow in the apex during suturing of the collateral vessels from the left circumflex artery (LCX) was calculated according to the formula: time flow = tissue counts × (reference flow/reference counts) and was expressed in milliliters per gram per minute (20).

Detection of H_2O_2 and NO production. 2′,7′-Dichlorodihydrofluorescein diacetate (DCF, Molecular Probes, Eugene, OR) and diaminorhodamine-4M AM (DAR, Daiichi Pure Chemicals, Tokyo) were used to detect H_2O_2 and NO production in coronary microvessels without a different NO scavenger (e.g., methylene blue), respectively, as previously described (21). Briefly, fresh and unfixed heart tissue was cut into several blocks and frozen in optimal cutting temperature compound (Tissue-Tek, Sakura Fine Chemical, Tokyo) within a few hours. Fluorescent images of [illegible] after application of ACh by using [illegible] pus BX51, Tokyo) (21). We used different animals for the fluorescent treatment (DCF and DAR) and the 2,3,5-triphenyltetrazolium chloride (TTC) treatment.

Western blotting. Portions of myocardial samples were homogenized in lysis buffer. After centrifugation, the supernatants were used for Western immunoblotting. The proteins were transferred by semidry electroblotting to polyvinylidene difluoride membranes. The blots were then blocked and incubated with horseradish peroxidase-conjugated rabbit anti-endothelial NO synthase (eNOS, dimer form) polyclonal antibody (Santa Cruz Biotechnology, Santa Cruz, CA) or anti-actin antibody (Santa Cruz Biotechnology). The antibody was visualized by using an enhanced chemiluminescence method (ECL; Amersham Biosciences, Tokyo). The integrated density of the bands was quantified by using NIH Image analysis, and the protein expression level of eNOS was normalized to that of actin (24).

Experimental protocols. After the surgical procedure and instrumentation, at least 30 min was allowed for stabilization while hemodynamic variables were monitored. The following protocols were examined.

Coronary vascular responses to endothelium-dependent [ACh, 0.5 and 1.0 μg/kg intracoronary (ic)] and -independent [sodium nitroprusside (SNP), 40 and 80 μg/min ic] vasodilators were examined before ischemia (90 min)-reperfusion (60 min) (I/R). ACh and SNP were continuously and retrogradely infused into the diagonal branch of the LAD by using a syringe pump (STC 525, Terumo, Tokyo). The coronary vascular responses to ACh and SNP were examined for 2 min, and the image of maximal vasodilatation was taken at 2 min of infusion of ACh or SNP.

Coronary vasodilator responses to ACh and SNP were examined before and after coronary ischemia (90 min)-reperfusion (60 min) by proximal LAD occlusion under the following seven conditions with cyclooxygenase blockade (ibuprofen, 12.5 mg/kg iv) to evaluate the [illegible] and NO without PGI_2 in a different set of animals (Fig. [illegible] N^G-monomethyl-L-arginine (L-NMMA) [illegible] and 240,000 U·kg [illegible] ic for 10 min, an inhibitor of H_2O_2 into water and oxygen), *4*) adenosine receptor blockade alone [8-sulfophenyltheophylline (8-SPT), 25 $\mu g \cdot kg^{-1} \cdot min^{-1}$ ic for 5 min], *5*) catalase plus L-NMMA, *6*) catalase plus tetraethylammonium [TEA, 10 $\mu g \cdot kg^{-1} \cdot min^{-1}$ ic for 10 min, an inhibitor of large-

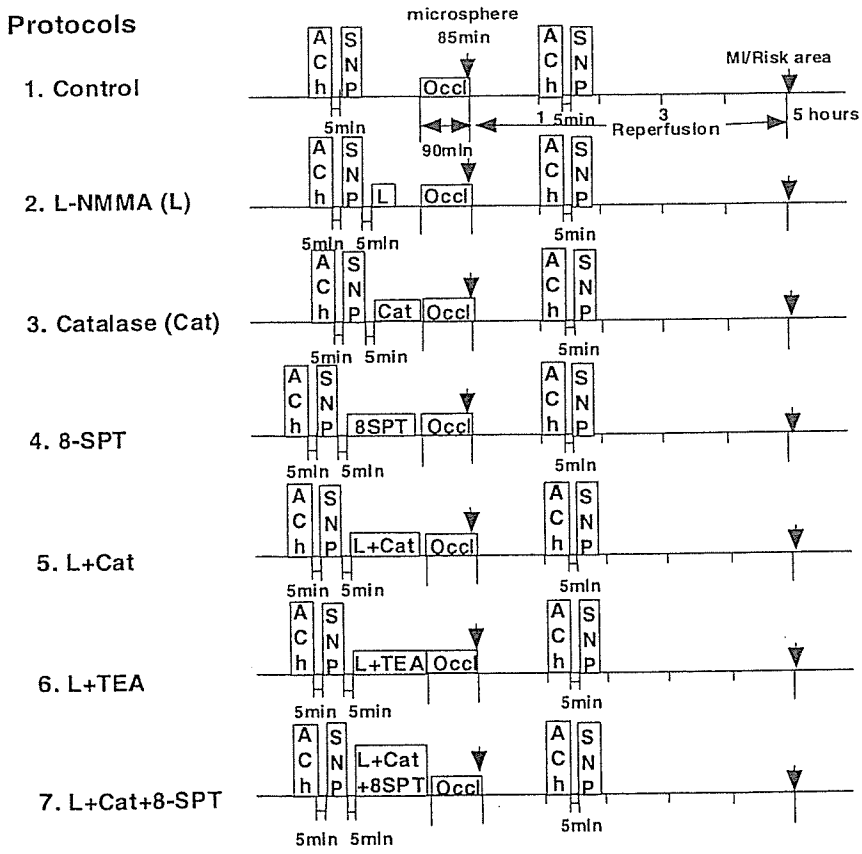

Fig. 1. Experimental protocols. TEA, tetraethylammonium; 8-SPT, 8-sulfophenyltheophylline; ACh, acetylcholine; SNP, sodium nitroprusside; Occl, coronary occlusion; Cat, catalase; L-NMMA (L), N^G-monomethyl-L-arginine; MI, myocardial infarction.

Table 1. *Hemodynamics during coronary ischemia-reperfusion injury in dogs*

		Before I/R			Ischemia (85 min)	After I/R		
	n	Baseline	ACh	SNP		Baseline	ACh	SNP
MBP, mmHg								
Control	5	92±4	91±6	92±5	93±14	92±4	91±5	92±6
L-NMMA	5	97±8	98±7	94±9	92±10	97±7	98±8	95±8
Cat	5	96±8	92±8	94±9	92±9	96±7	96±8	98±6
L-NMMA + Cat	5	94±4	93±9	97±9	95±11	95±8	98±5	94±5
L-NMMA + TEA	5	95±12	93±13	95±14	94±10	91±14	93±15	98±10
L-NMMA + Cat + 8-SPT	5	95±3	96±4	95±3	93±11	96±3	97±4	95±3
Heart rate, beats/min								
Control	5	152±5	155±3	154±3	156±7	156±5	154±5	153±5
L-NMMA	5	157±5	156±5	157±6	158±6	153±5	153±5	153±5
Cat	5	155±4	159±6	158±5	157±6	151±7	155±8	154±8
L-NMMA + Cat	5	156±12	158±13	158±13	154±5	156±13	156±14	159±13
L-NMMA + TEA	5	153±13	154±12	155±11	155±5	150±10	151±11	152±10
L-NMMA + Cat + 8-SPT	5	152±7	155±9	153±3	153±5	152±7	151±6	153±7

Results are expressed as means ± SE; n = no. of dogs. I/R, ischemia-reperfusion; MBP, mean blood pressure; Cat, catalase; SNP, sodium nitroprusside; TEA, tetraethylammonium; 8-SPT, sulfophenyltheophylline; L-NMMA, N^G-monomethyl-L-arginine.

conductance Ca^{2+}-sensitive potassium (K_{Ca}) channels], and *7*) catalase plus L-NMMA with 8-SPT (35). These inhibitors were given at 30 min before I/R. An interval between each treatment was 5 min. The basal coronary diameter was defined as that before administration of ACh or SNP either before or after I/R. L-NMMA, catalase, TEA, and 8-SPT were administered alone at 5 min after administration of ACh or SNP. Microspheres were administered at 85 min after the initiation of coronary occlusion. In the combined infusion (L-NMMA + catalase + 8-SPT), catalase solution was infused into the LAD at a rate of 0.5 ml/min at 5 min after infusion of L-NMMA, and then 8-SPT was added into the LAD at 15 min after the initiation of L-NMMA.

After 1 h of reperfusion, coronary vasodilator responses to ACh and SNP were examined.

After 5 h of reperfusion, we reoccluded the LAD and injected Evans blue dye into a systemic vein. Then, myocardial slices (5 μm thick) were incubated in 1% TTC (Sigma) solution to detect the infarct area (36). Different animals were used for fluorescent treatment (DCF and DAR) and TTC treatment.

Drugs. All drugs were obtained from Sigma Chemical and were diluted in a physiological saline immediately before use.

Statistical analysis. Results are expressed as means ± SE. Vascular responses (see Figs. 3*C*, 5*F*, 6*F*, 7, and 9*A*) were analyzed by one-way ANOVA followed by Scheffé's post hoc test for multiple comparisons. Difference in the effects of ACh and SNP on subepicardial coronary microvessels before and after I/R (see Figs. 3, *A* and *B*, 4, and 8, *A* and *B*), and difference between infarct size/risk area and transmural collateral flow in control and other inhibitors (see Fig. 9*B*) were examined by a multiple regression analysis by using a model in which the change in coronary diameter was set as a dependent variable (y) and vascular size as an explanatory variable (x), while the statuses of control and other inhibitors were set as dummy variables (D_1, D_2) in the following equation: $y = a_0 + a_1x + a_2D_1 + a_3D_2$, where a_0 through a_3 are partial regression coefficients (36). The criterion for statistical significance was at $P < 0.05$.

RESULTS

Hemodynamics and blood gases during I/R injury. Immediately after reperfusion, coronary blood flow was increased and some arrhythmias occurred; however, those changes returned to the control levels 1 h after reperfusion when we repeated the measurements. Thus, throughout the experiments, mean aortic pressure and heart rate at baseline were constant and comparable, and Po_2, Pco_2, and pH were maintained within the physiological ranges (pH 7.35–7.45, Po_2 > 70 mmHg, and Pco_2 25–40 mmHg,). Hemodynamic variables at baseline did not significantly change after I/R compared with those before I/R (Tables 1 and 2).

Dose responses to ACh and SNP. ACh (0.5 and 1.0 μg/kg ic) and SNP (40 and 80 μg/min ic) caused coronary vasodilatation in a dose-dependent manner at both small arteries and arterioles (Fig. 2). Then we chose the maximal dose of the vasodilators (ACh, 1.0 μg/kg ic, and SNP, 80 μg/min ic) in the following experiments.

Endothelium-dependent coronary vasodilatation before and after I/R. There was no significant difference in baseline diameter after ACh before I/R among the groups. All inhibitors did not affect resting coronary artery diameter or coronary

Table 2. *Baseline vascular diameter before I/R in response to ACh*

	Small Artery	Arteriole
Control	104–150 μm (120±7, n = 7)	37–96 μm (70±6, n = 12)
L-NMMA	106–164 μm (131±7, n = 8)	36–95 μm (63±5, n = 16)
Cat	100–147 μm (121±5, n = 10)	28–89 μm (61±6, n = 12)
8-SPT	114–162 μm (130±8, n = 6)	30–88 μm (60±10, n = 5)
L-NMMA + Cat	102–141 μm (118±5, n = 8)	34–95 μm (77±4, n = 10)
L-NMMA + TEA	105–142 μm (123±6, n = 5)	34–95 μm (62±9, n = 8)
L-NMMA + Cat + 8-SPT	110–145 μm (128±6, n = 5)	38–87 μm (67±7, n = 7)

Results are expressed as range (means ± SE); n = no. of blood vessels.

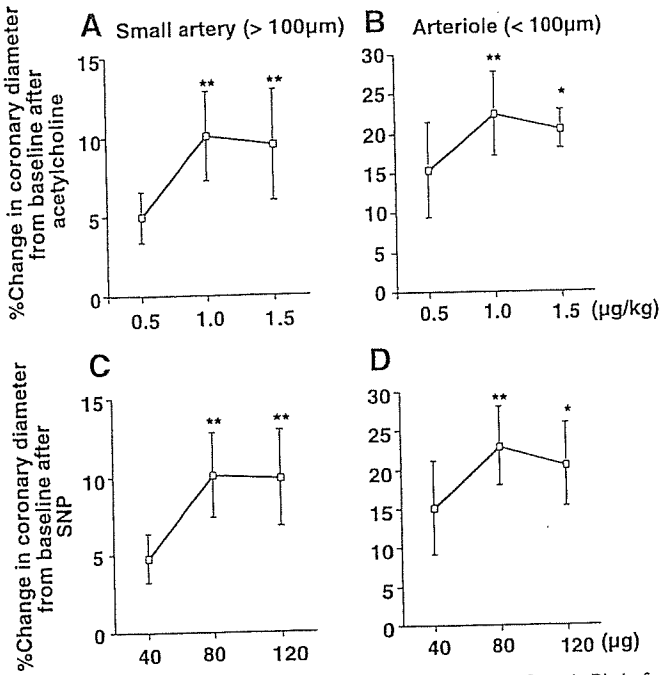

Fig. 2. Dose responses to ACh (*A* and *B*) and SNP (*C* and *D*) before ischemia-reperfusion (I/R). Number of small arteries (*A* and *C*) and arterioles (*B* and *D*) per animals used was 5/5 for each group. $*P < 0.05$, $**P < 0.01$ vs. ACh (0.5 μg/kg) and SNP (40 μg).

blood flow. Under control conditions (before I/R), intracoronary administration of ACh caused a significantly greater coronary vasodilatation in arterioles than in small arteries (Fig. 3, *A* and *B*). Coronary I/R significantly impaired the coronary vasodilatation to ACh in both sized arteries (Figs. 3*A* and 4*A*), and L-NMMA reduced the vasodilatation in small arteries (Figs. 3*A* and 4*B*) but rather increased the response in arterioles compared with control (Figs. 3*B* and 4*A*) after I/R. Catalase and 8-SPT increased the ACh-induced vasodilatation in small arteries (Figs. 3*A* and 4, *C* and *D*) but decreased the response in arterioles (Fig. 3*B*) after I/R. There was no significant difference in coronary blood flow before and after I/R among the control, the L-NMMA, and the catalase group (Fig. 3*C*). L-NMMA + catalase (Figs. 3, *A* and *B*, and 4*E*) or L-NMMA + TEA (Figs. 3, *A* and *B*, and 4*F*) decreased the vasodilatation in both sized arteries (Fig. 3, *A* and *B*) with decrement of coronary blood flow (Fig. 3*C*), and L-NMMA plus catalase with 8-SPT further decreased the vasodilatation in both sized arteries (Figs. 3, *A* and *B*, and 4*G*) compared with other groups (Fig. 3, *A–C*).

Detection of H_2O_2 and NO production. Fluorescent microscopy with DCF showed that I/R increased the vascular H_2O_2 production in control LCX (Fig. 5, *B* and *F*) compared with baseline conditions (Fig. 5, *A* and *F*) and decreased the H_2O_2 production in control LAD (Figs. 5, *C* and *F*), which was enhanced by L-NMMA (Fig. 5, *D* and *F*) and was abolished by catalase (Fig. 5, *E* and *F*) in arterioles. By contrast, the production of NO as assessed with DAR fluorescence was increased in control LCX (Fig. 6, *B* and *F*) compared with baseline LCX (Fig. 6, *A* and *F*) after I/R, decreased in control LAD (Fig. 6, *C* and *F*), inhibited by L-NMMA (Fig. 6, *D* and *F*), and was enhanced by catalase (Fig. 6, *E* and *F*) in small arteries.

Western blotting of eNOS protein expression in myocardium. In the control group, expression of eNOS protein in the ischemic LAD area was significantly decreased compared with the nonischemic LCX area (Fig. 7). In the catalase group, this decrease in the eNOS protein expression was inhibited by catalase (Fig. 7).

Endothelium-independent coronary vasodilatation. Coronary vasodilator responses to SNP were comparable under all conditions in both sized arteries (Fig. 8). Those coronary vasodilator responses were resistant to the blockade of NO synthesis with L-NMMA (Fig. 8).

Effect of H_2O_2 on I/R-induced myocardial infarct size. I/R injury caused myocardial infarction, the size of which was ~40% of the LV risk area (Fig. 9*A*). Intracoronary L-NMMA, catalase, or 8-SPT alone did not further increase the I/R-induced infarct size (Fig. 9*A*). By contrast, intracoronary L-NMMA plus catalase or TEA markedly increased the infarct size, and L-NMMA plus catalase with 8-SPT further increased

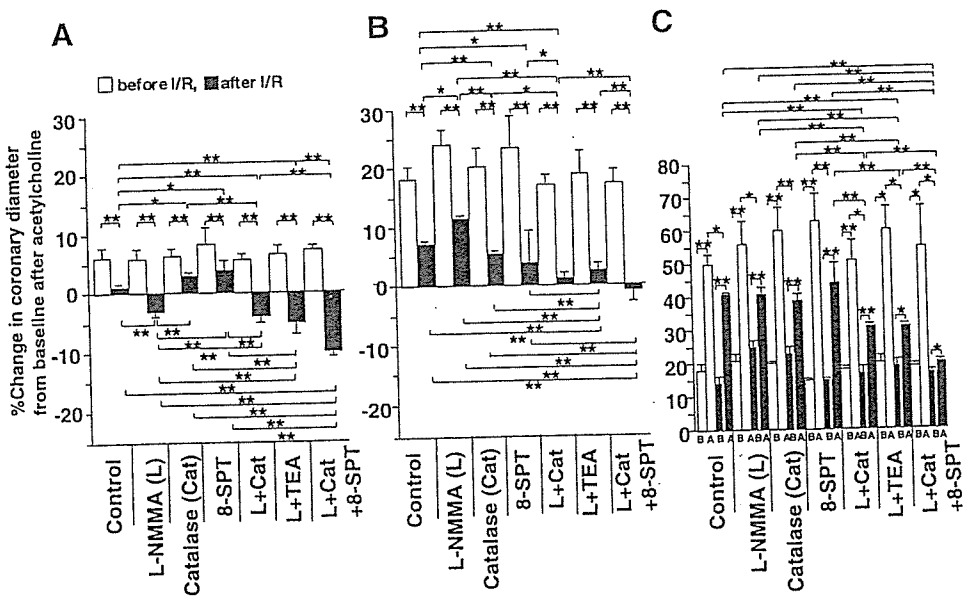

Fig. 3. Endothelium-dependent coronary vasodilatation to ACh before and after coronary I/R injury in dogs in vivo. *A*: small artery (≥100 μm). *B*: arteriole (<100 μm). *C*: coronary blood flow (CBF). No. of small arteries or arterioles per animals (*n/n*) used was 7/5 for control, 8/5 for L-NMMA, 10/5 for catalase, 6/5 for 8-SPT, 8/5 for L-NMMA plus catalase, 5/5 for L-NMMA plus TEA, and 5/5 for L-NMMA plus catalase plus 8-SPT in small arteries; and 12/5 for control, 16/5 for L-NMMA, 12/5 for catalase, 5/5 for 8-SPT, 10/5 for L-NMMA plus catalase, 8/5 for L-NMMA plus TEA, and 7/5 for L-NMMA plus catalase plus 8-SPT in arterioles. No. of animals during the measuring CBF used was 5 for each group. B, before ACh; A, after ACh. $*P < 0.05$, $**P < 0.01$.

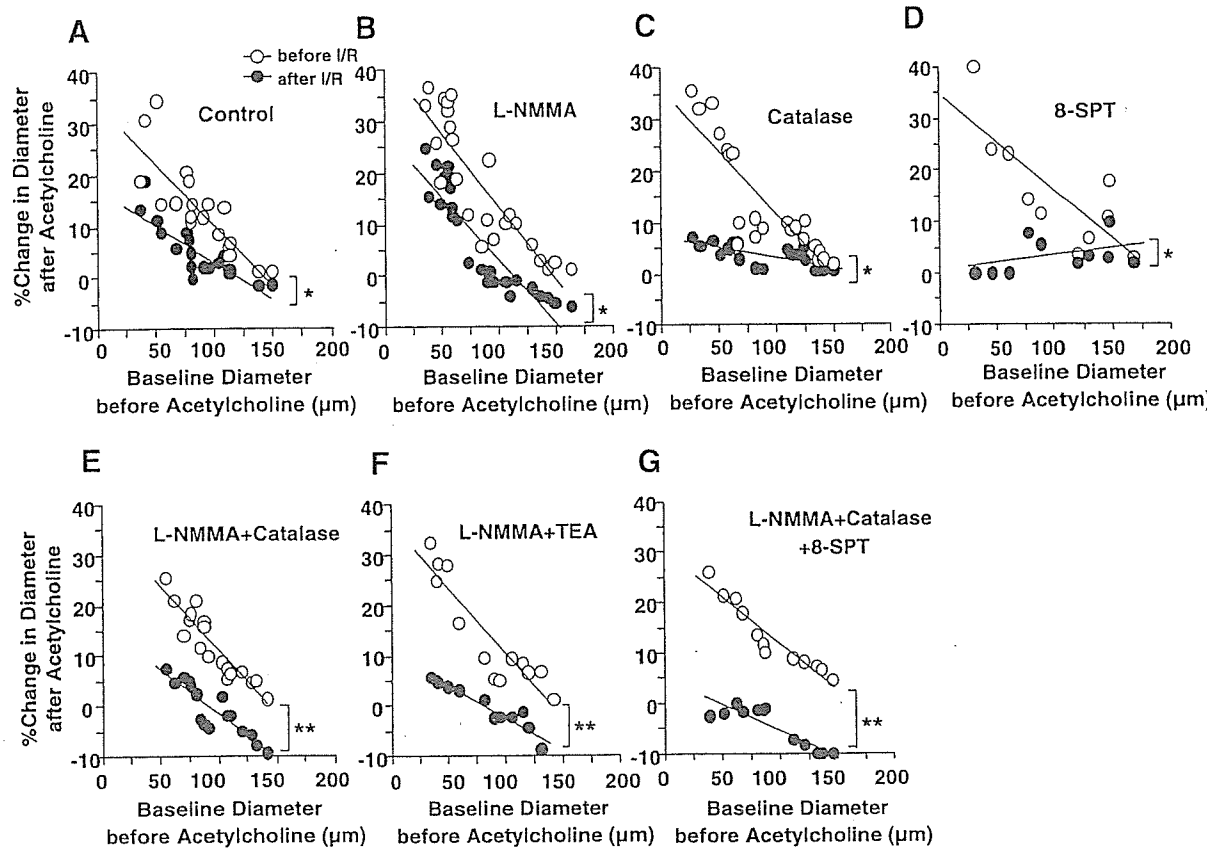

Fig. 4. Percent change in diameter after ACh before and after coronary I/R injury in dogs in vivo. No. of small arteries and arterioles per animals used was 7/5 for control (*A*), 8/5 for L-NMMA (*B*), 10/5 for catalase (*C*), 6/5 for 8-SPT (*D*), 8/5 for L-NMMA plus catalase (*E*), 5/5 for L-NMMA plus TEA (*F*), and 5/5 for L-NMMA plus catalase plus 8-SPT in small arteries (*G*); and 12/5 for control (*A*), 16/5 for L-NMMA (*B*), 12/5 for catalase (*C*), 5/5 for 8-SPT (*D*), 10/5 for L-NMMA plus catalase (*E*), 8/5 for L-NMMA plus TEA (*F*), and 7/5 for L-NMMA plus catalase plus 8-SPT in arterioles (*G*). $^*P < 0.05$, $^{**}P < 0.01$.

the infarct size (Fig. 9*A*). In the control group, there was an inverse relation between the infarct size and transmural collateral blood flow measured by microsphere technique ($r = 0.90$, $P < 0.01$). There was no significant difference in the relationship among the control, L-NMMA, and catalase treatment (Fig. 9*B*). L-NMMA plus catalase or TEA significantly shifted the regression line upward compared with the control group (both $P < 0.01$), and L-NMMA plus catalase with 8-SPT further shifted the regression line upward compared with L-NMMA plus catalase or TEA (Fig. 9*B*, both $P < 0.01$).

DISCUSSION

The major finding of the present study is that endogenous H_2O_2, in cooperation with NO, plays an important cardioprotective role during coronary I/R injury as a compensatory mechanism for NO in vivo. To the best of our knowledge, this is the first report that demonstrates the important protective role of endogenous H_2O_2, in cooperation with NO, against coronary I/R injury in vivo.

Validations of experimental model and methodology. On the basis of the previous reports (22, 31), we chose the adequate dose of ACh, SNP, L-NMMA, catalase, TEA, and 8-SPT to examine the effects of endothelium-dependent and -independent coronary vasodilator responses and inhibition of NO synthesis, H_2O_2, K_{Ca} channels, and adenosine receptor, respectively. In addition, on the basis of previous studies and our own (31, 35), we choose the doses of ACh and SNP that cause maximal coronary vasodilatation in dogs in vivo. TEA at low doses is fairly specific for K_{Ca} channel, but at higher doses it may block a number of other K channels. Because several K_{Ca} channels are involved in H_2O_2-mediated responses (26), we selected the nonselective K_{Ca} inhibitor TEA to inhibit all K_{Ca} channels (15). We have previously confirmed the validity of the methods that we used in the present study (32). After 60–90 min of ischemia, ultrastructural damage of coronary endothelium was observed particularly in the subendocardium in the present study, a finding consistent with the previous study (8).

H_2O_2 during coronary I/R in vivo. It was previously reported that relaxations of isolated large canine coronary arteries to exogenous H_2O_2 were partially endothelium dependent (23). Recently, Matoba et al. (16, 17) identified that endothelium-derived H_2O_2 is an EDHF in mouse and human mesenteric microvessels. Subsequently, we (35) and others (19) have confirmed that endogenous H_2O_2 exerts important vasodilator effects in canine coronary microcirculation in vivo and in isolated human coronary microvessels, respectively. It is conceivable that H_2O_2 is produced from superoxide anions derived from several sources in endothelial cells, including eNOS, cyclooxygenase, lipoxygenase, cytochrome *P*-450 enzymes, and NAD(P)H oxidases (16). In the present study, L-NMMA or catalase alone did not com-

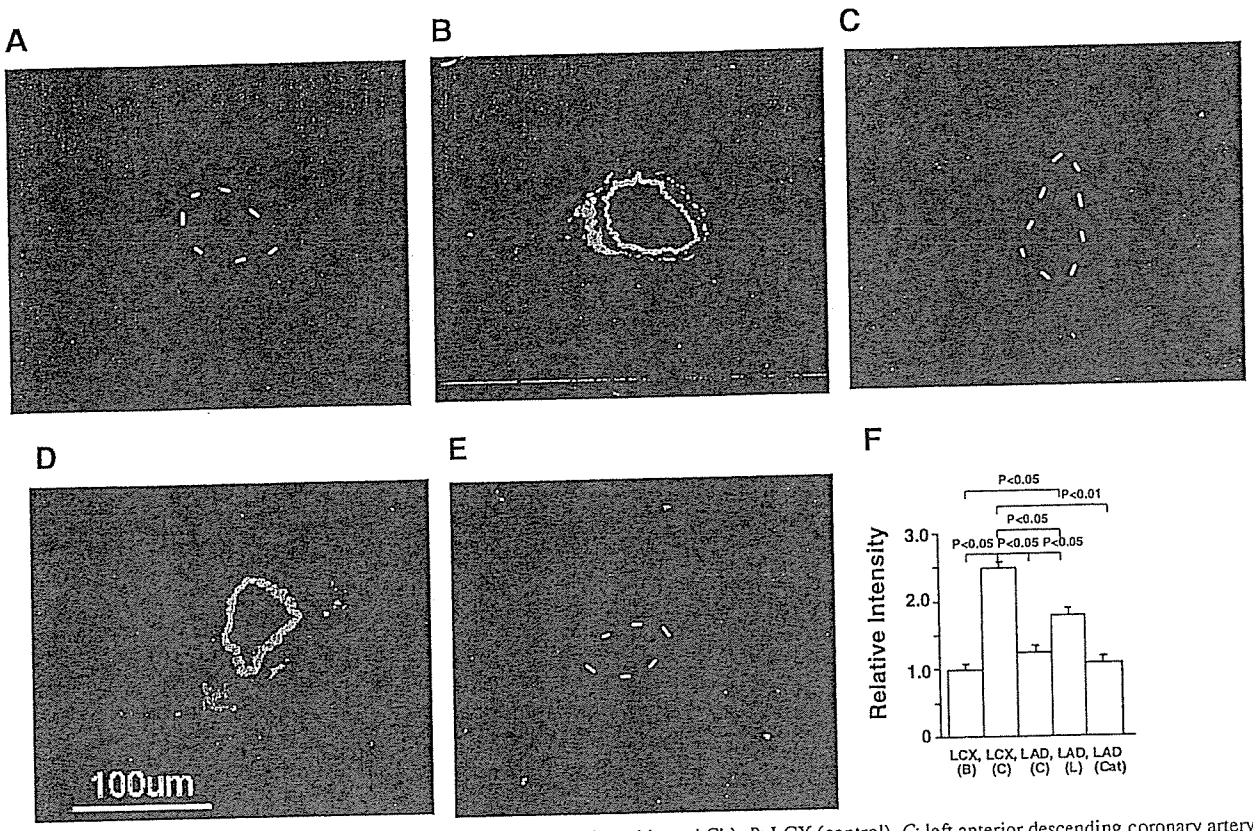

Fig. 5. Detection of H_2O_2 production. *A*: left circumflex artery (LCX; baseline without ACh). *B*: LCX (control). *C*: left anterior descending coronary artery (LAD; control). *D*: LAD (L-NMMA). *E*: LAD (catalase). *F*: fluorescent intensity (B, baseline without ACh; C, control, L, L-NMMA; Cat, catalase). No. of arterioles per animals used was 5/5 for each group. Dashed line, outline of vessels. Bar, 100 μm.

pletely abolish the ACh-induced vasodilatation in both sized arteries, whereas L-NMMA plus catalase markedly attenuated the residual vasodilatation in vivo as did TEA, indicating that H_2O_2 exerts important vasodilator effects during I/R injury in canine coronary microcirculation in vivo (Figs. 3 and 4). Furthermore, in the present study, endogenous H_2O_2-mediated coronary vasodilatation was noted to a greater extent in arterioles than in small arteries (Figs. 3 and 4), confirming the predominant role of H_2O_2 in microvessels and that of NO in relatively large arteries in vivo (25).

Compensatory vasodilator mechanism among H_2O_2, NO, and adenosine. It is well known that coronary vascular tone is regulated by the interactions among several endogenous vasodilators, including NO, H_2O_2, and adenosine (33). These vasodilators play an important role in compensatory vasodilatation of coronary microvessels during myocardial ischemia (35). In the present study (Figs. 3 and 4), endothelium-dependent arteriolar vasodilatation to ACh during coronary I/R was significantly increased by L-NMMA while small arterial vasodilatation to ACh was increased by catalase and 8-SPT, and the residual arteriolar dilation was further inhibited by both of them (L-NMMA plus catalase or TEA). Furthermore, fluorescent microscopy with DCF and DAR, respectively, showed that H_2O_2 and NO production after I/R were enhanced in small coronary arteries and arterioles by L-NMMA [fluorescent intensity (FI) 1.8] and catalase (FI 1.9) compared with those in the LAD of control group (Figs. 5 and 6, FI: DAR 1.2 and DCF 1.1). The residual small arteriolar dilatation after combined administration of L-NMMA + catalase was completely blocked by 8-SPT, an adenosine receptor blocker, indicating that adenosine also compensated for the loss of action of NO and H_2O_2. Taken together, these results indicate the compensatory vasodilator effects among NO, H_2O_2, and adenosine to maintain coronary blood flow during coronary I/R injury in vivo. H_2O_2 and NO were mutually compensatory in both small arteries and arterioles, and in the presence of their inhibitors (catalase and L-NMMA), adenosine also caused arteriolar vasodilatation, as we reported previously (35). This finding is consistent with our finding that NO, H_2O_2, and adenosine play an important compensatory role in coronary autoregulation in canine coronary microcirculation in vivo (35). It was reported that TEA inhibited adenosine-induced vasodilatation of canine subepicardial coronary arteries in vitro (3). Furthermore, H_2O_2 stimulates protein kinase C, phospholipase A_2, and arachidonic acid release and increases intracellular cAMP levels (10). These findings suggest that cAMP-mediated pathway is involved, at least in part, during coronary vasodilatation through K_{Ca} channels after I/R injury.

Role of H_2O_2 during coronary I/R. It is known that K_{Ca} channels substantially contribute to coronary vasodilatation in myocardial ischemia (22) and that H_2O_2 also activates K_{Ca} channels (11). However, it remains to be examined whether H_2O_2 contributes to coronary vasodilatation during I/R in vivo. The present results demonstrate that H_2O_2

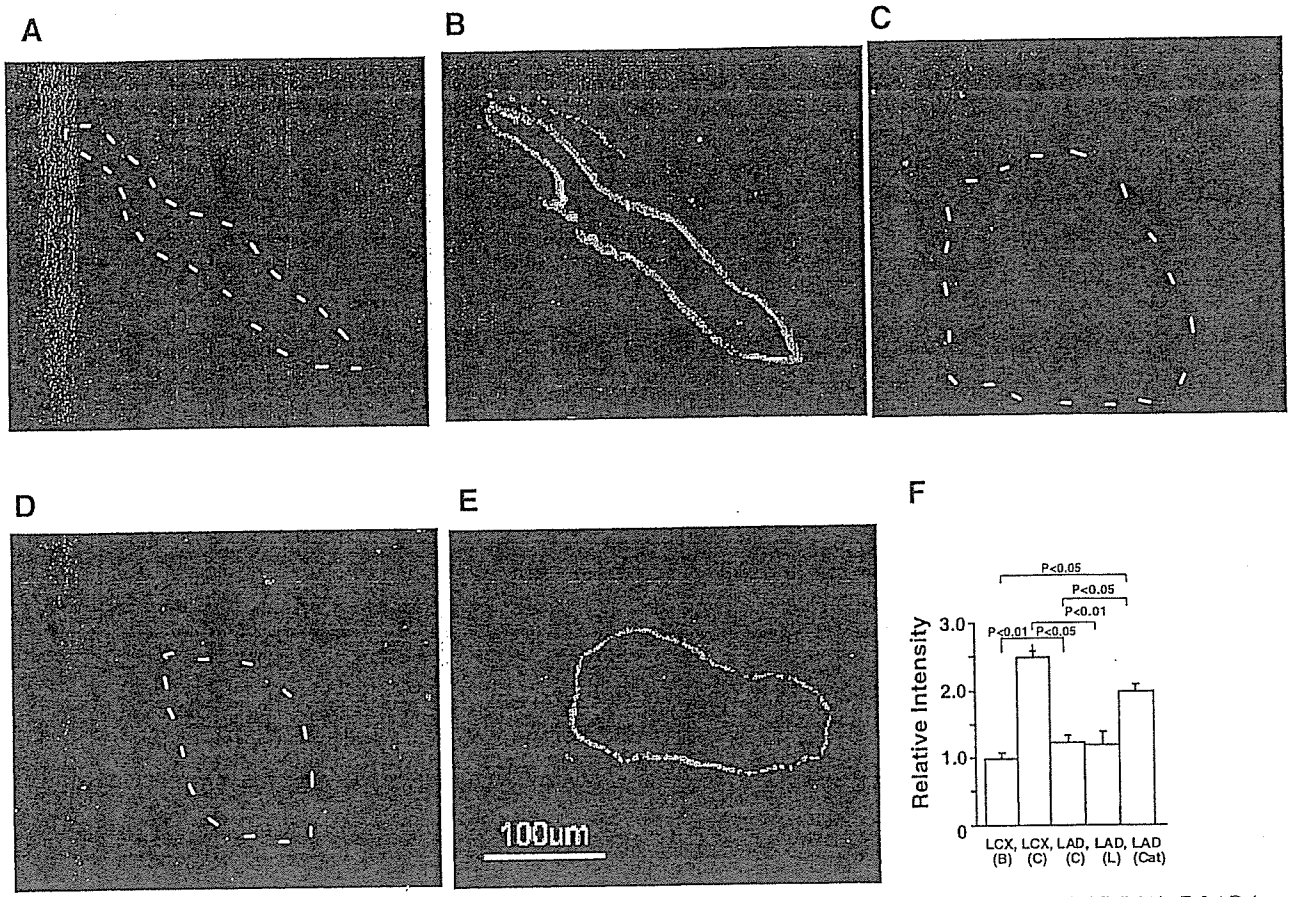

Fig. 6. Detection of nitric oxide (NO) production. *A*: LCX (baseline without ACh). *B*: LCX (control). *C*: LAD (control). *D*: LAD (L-NMMA). *E*: LAD (catalase). *F*: fluorescent intensity (B, baseline without ACh; C, control, L, L-NMMA; Cat, catalase). No. of small arteries per animals used was 5/5 for each group. Dashed line, outline of vessels.

substantially contributes to coronary vasodilatation during I/R in vivo as a compensatory mechanism for the loss of NO. Several mechanisms have been proposed for K_{Ca} channel opening during coronary I/R, including cellular acidosis

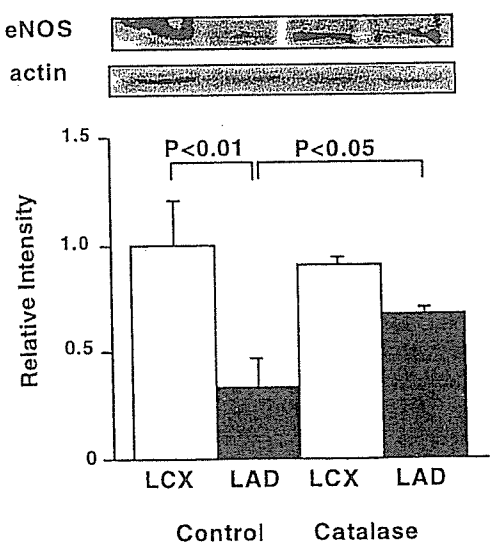

Fig. 7. Western blotting showing the effects of catalase on endothelial nitric oxide synthase (eNOS) protein expression in the myocardium of LAD and LCX. No. of animals used was 3 for each group.

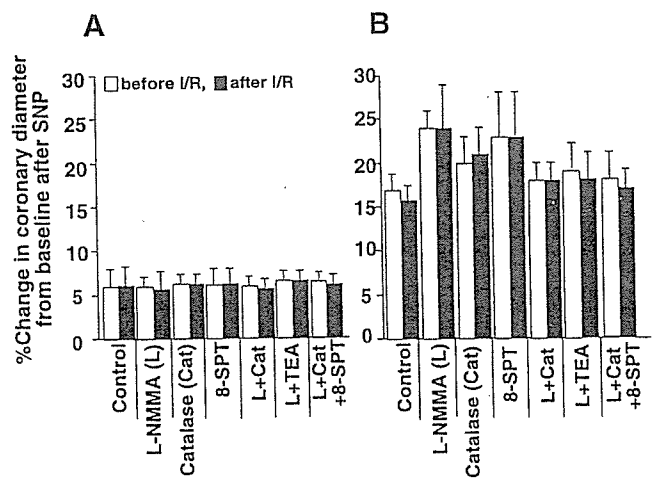

Fig. 8. Endothelium-independent coronary vasodilatation before and after coronary I/R injury in dogs in vivo. *A*: small artery (≥100 μm). *B*: arteriole (<100 μm). No. of small arteries and arterioles per animals used (*n*/*n*) was 7/5 for control, 8/5 for L-NMMA, 10/5 for catalase, 6/5 for 8-SPT, 8/5 for L-NMMA plus catalase, 5/5 for L-NMMA plus TEA, and 5/5 for L-NMMA plus catalase plus 8-SPT in small arteries; and 12/5 for control, 16/5 for L-NMMA, 12/5 for catalase, 5/5 for 8-SPT, 10/5 for L-NMMA plus catalase, 8/5 for L-NMMA plus TEA, and 7/5 for L-NMMA plus catalase plus 8-SPT in arterioles.

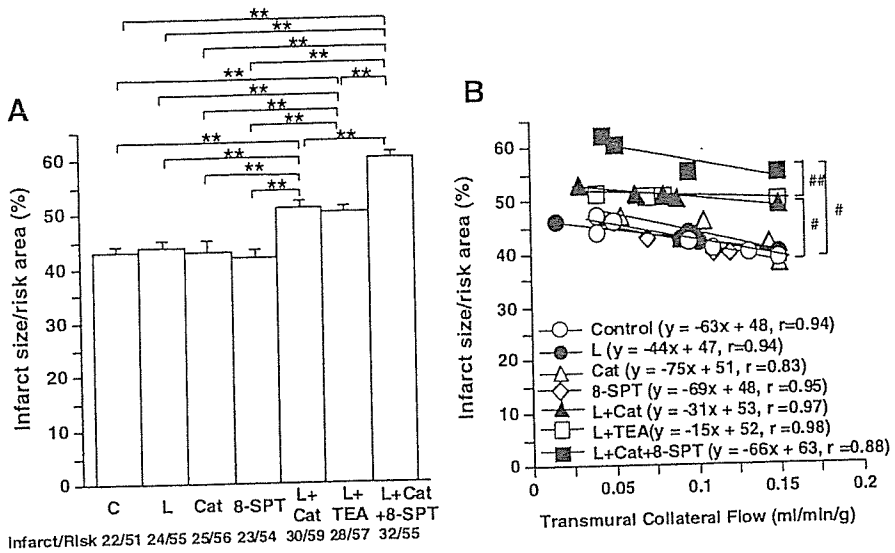

Fig. 9. Effects of H_2O_2, NO, and adenosine on I/R-induced MI in dogs in vivo. *A*: I/R-induced left ventricular infarct size in dogs in vivo. C, control. *B*: plot of infarct size expressed as a percentage of the risk area and regional collateral flow during I/R. $^{**}P < 0.01$, $\#P < 0.05$ vs. L-NMMA (L) or Cat or 8-SPT; $\#\#P < 0.01$ vs. L + TEA or L + Cat.

(27), increase in intracellular Ca^{2+} concentration after ischemia (28), and H_2O_2 production by inflammatory cells (5). Furthermore, an inhibitor of NO synthesis [N^G-nitro-L-arginine methyl ester (L-NAME)] or that of K_{Ca} channels (charybdotoxin) partly inhibits the protective effect on myocardial infarct size (22). Liu et al. (14) demonstrated that peroxynitrite inhibits K_{Ca} channel activity in human coronary arterioles during I/R. This mechanism might contribute to impaired H_2O_2-mediated dilation in I/R where NO synthase activity is increased in the presence of excess of O_2^-. In the present study, inhibition of H_2O_2 or NO alone did not significantly increase myocardial infarct size compared with control conditions (Fig. 9). These results suggest that H_2O_2 and NO exert cardioprotective effects against the development of myocardial infarction in a compensatory manner.

Recently, we have demonstrated that the expression of eNOS protein is decreased in the ischemic myocardium, which is improved by a selective Rho-kinase inhibitor, hydroxyfasudil, during coronary I/R injury in dogs in vivo (36). Furthermore, a physiological concentration (2 μmol/l) of H_2O_2 improved the recovery of both cardiac contractile function and energy metabolism after I/R in perfused rat heart (37). In the present study, the expression of eNOS protein was decreased in the ischemic myocardium, which was increased by catalase during I/R injury (Fig. 7). All these mechanisms may be involved in the beneficial effects of H_2O_2 on the I/R-induced myocardial injury. It also is conceivable that I/R reduces endothelial tetrahydrobiopterin levels in coronary vessels and impairs eNOS function (30).

Limitations of the study. Several limitations should be mentioned for the present study. First, we did not examine coronary vasodilatation in response to SOD/SOD mimetic (e.g., Tempol) or peroxynitrite inhibitor (e.g., ebselen) after I/R. However, because of the complex interactions among the oxygen species, we consider that both Tempol and ebselen also affect H_2O_2 metabolism by scavenging superoxide anions and peroxynitrite, respectively. Second, in addition to catalase, endogenous glutathione peroxidase (GSH) also plays an important role in removing H_2O_2, and NO also could be a substrate for endogenous catalase (1). However, in the present study, we used exogenous catalase to remove H_2O_2 to examine the role of the reactive oxygen species. Third, the exact source of vascular H_2O_2 production remains to be elucidated (e.g., the endothelium, smooth muscle, or cardiomyocytes). Fourth, while we were able to demonstrate the production of H_2O_2 using fluorescent microscopy with DCF, we were unable to quantitatively measure the H_2O_2 production because DCF detects H_2O_2, $ONOO^-$, and HOCl as well. Fifth, we were unable to find smaller arterioles because of the limited spatial resolution of our CCD intravital microscope. If we had an intravital camera with higher resolution, we would be able to observe coronary vasodilator responses of smaller arterioles.

Clinical implications and conclusions. During coronary I/R, microemboli of atherosclerosis debris and platelet plugs are released into the coronary microcirculation, particularly at revascularization with thrombolysis and/or percutaneous coronary intervention. Thus preexisting coronary endothelial dysfunction with various risk factors may be an important determinant for I/R injury in acute myocardial infarction. The synthesis and/or action of endothelium-derived NO are impaired under various pathological conditions, such as hypertension, hyperlipidemia, and diabetes mellitus (26, 34). In hypertension, K channel activities are increased in a compensatory manner with reduced NO activity (13). The present results suggest that NO and H_2O_2 compensate each other to cause coronary vasodilatation during I/R injury in vivo.

In conclusion, we were able to demonstrate that endogenous H_2O_2, in cooperation with NO, plays an important cardioprotective role in coronary I/R injury in vivo. The present findings may have important clinical implications because H_2O_2-mediated mechanisms substantially contribute to endothelium-dependent vasodilatation in coronary I/R in vivo.

GRANTS

This work was supported in part by grants from the Japanese Ministry of Education, Science, Sports, Culture, and Technology, Tokyo, Japan (Nos. 13307024, 13557068, 14657178, 15256003, 16209027, 16300164), and the Program for Promotion of Fundamental Studies in Health Sciences of the Organization for Pharmaceutical Safety and Research of Japan.

REFERENCES

1. Antunes F, Han D, and Cadenas E. Relative contributions of heart mitochondria glutathione peroxidase and catalase to H_2O_2 detoxification in in vivo conditions. *Free Radic Biol Med* 33: 1260–1267, 2002.
2. Bauersachs J, Hecker M, and Busse R. Display of the characteristics of endothelium-derived hyperpolarizing factor by a cytochrome *P*450-derived arachidonic acid metabolite in the coronary microcirculation. *Br J Pharmacol* 113: 1548–1553, 1994.
3. Cabell F, Weiss DS, and Price JM. Inhibition of adenosine-induced coronary vasodilation by block of large-conductance Ca^{2+} activated K^+ channels. *Am J Physiol Heart Circ Physiol* 267: H1455–H1460, 1994.
4. Campbell WB, Gebremedhin D, Pratt PF, and Harder DR. Identification of epoxyeicosatrienoic acids as an endothelium-derived hyperpolarizing factor. *Circ Res* 78: 415–423, 1996.
5. Chandrasekar B, Colston JT, de la Rosa SD, Rao PP, and Freeman GL. TNF-α and H_2O_2 induce IL-18 and IL-18R β expression in cardiomyocytes via NF-κB activation. *Biochem Biophys Res Commun* 303: 1152–1158, 2003.
6. Chen G, Suzuki H, and Weston AH. Acetylcholine releases endothelium-derived hyperpolarizing factor and EDRF from blood vessels. *Br J Pharmacol* 95: 1165–1174, 1988.
7. Edwards G, Dora KA, Gardener MJ, Garland CJ, and Weston AH. K^+ is an endothelium-derived hyperpolarizing factor in rat arteries. *Nature* 396: 269–272, 1998.
8. Ehring T, Krajcar M, Baumgart D, Kompa S, Hummelgen M, and Heusch G. Cholinergic and α-adrenergic coronary constriction with increasing ischemia-reperfusion injury. *Am J Physiol Heart Circ Physiol* 268: H886–H894, 1995.
9. Feletou M and Vanhoutte PM. Endothelium-dependent hyperpolarization of canine smooth muscle. *Br J Pharmacol* 93: 515–524, 1988.
10. Gao Y and Vanhoutte PM. Effects of hydrogen peroxide on the responsiveness of isolated canine bronchi: role of prostaglandin E_2 and I_2. *Am J Physiol Lung Cell Mol Physiol* 263: L402–L408, 1992.
11. Hayabuchi Y, Nakaya Y, Matsuoka S, and Kuroda Y. Hydrogen peroxide-induced vascular relaxation in porcine coronary arteries is mediated by Ca^{2+}-activated K^+ channels. *Heart Vessels.* 13: 9–17, 1998.
12. Huang A, Sun D, Carroll MA, Jiang H, Smith CJ, Connetta JA, Falck JR, Shesely EG, Koller A, and Kaley G. EDHF mediates flow-induced dilation in skeletal muscle arterioles of female eNOS-KO mice. *Am J Physiol Heart Circ Physiol* 280: H2462–H2469, 2001.
13. Liu Y, Hudetz AG, Knaus HG, and Rusch NJ. Increased expression of Ca^{2+}-sensitive K^+ channels in the cerebral microcirculation of genetically hypertensive rats: evidence for their protection against cerebral vasospasm. *Circ Res* 82: 729–737, 1998.
14. Liu Y, Terata K, Chai Q, Li H, Kleinman LH, and Gutterman DD. Peroxynitrite inhibits Ca^{2+}-activated K^+ channel activity in smooth muscle of human coronary arterioles. *Circ Res* 91: 1070–1076, 2002.
15. Masumoto A, Hirooka Y, Shimokawa H, Hironaga K, Setoguchi S, and Takeshita A. Possible involvement of Rho-kinase in the pathogenesis of hypertension in humans. *Hypertension* 38: 1307–1310, 2001.
16. Matoba T, Shimokawa H, Nakashima M, Hirakawa Y, Mukai Y, Hirano K, Kanaide H, and Takeshita A. Hydrogen peroxide is an endothelium-derived hyperpolarizing factor in mice. *J Clin Invest* 106: 1521–1530, 2000.
17. Matoba T, Shimokawa H, Kubota H, Morikawa K, Fujiki T, Kunihiro I, Mukai Y, Hirakawa Y, and Takeshita A. Hydrogen peroxide is an endothelium-derived hyperpolarizing factor in human mesenteric arteries. *Biochem Biophys Res Commun* 290: 909–913, 2002.
18. Mehta JL, Nichols WW, Donnelly WH, Lawson DL, and Saldeen TG. Impaired canine coronary vasodilator response to acetylcholine and bradykinin after occlusion-reperfusion. *Circ Res* 64: 43–54, 1989.
19. Miura H, Bosnjak JJ, Ning G, Saito T, Miura M, and Gutterman DD. Role for hydrogen peroxide in flow-induced dilation of human coronary arterioles. *Circ Res* 92: e31–e40, 2003.
20. Mori H, Haruyama Y, Shinozaki H, Okino H, Iida A, Takanashi R, Sakuma I, Husseini WK, Payne BD, and Hoffman JI. New nonradioactive microspheres and more sensitive X-ray fluorescence to measure regional blood flow. *Am J Physiol Heart Circ Physiol* 263: H1946–H1957, 1992.
21. Morikawa K, Shimokawa H, Matoba T, Kubota H, Akaike T, Talukder MA, Hatanaka M, Fujiki T, Maeda H, Takahashi S, and Takeshita A. Pivotal role of Cu,Zn-superoxide dismutase in endothelium-dependent hyperpolarization. *J Clin Invest.* 112: 1871–1879, 2003.
22. Ogita H, Node K, Asanuma H, Sanada S, Liao Y, Takashima S, Asakura M, Mori H, Shinozaki Y, Hori M, and Kitakaze M. Amelioration of ischemia- and reperfusion-induced myocardial injury by the selective estrogen receptor modulator, raloxifene, in the canine heart. *J Am Coll Cardiol* 40: 998–1005, 2002.
23. Rubanyi GM and Vanhoutte PM. Oxygen-derived radicals, endothelium, and responsiveness of vascular smooth muscle. *Am J Physiol Heart Circ Physiol* 250: H815–H821, 1986.
24. Satoh M, Fujimoto S, Haruna Y, Arakawa S, Horike H, Komai N, Sasaki T, Tsujioka K, Makino H, and Kashihara N. NAD(P)H oxidase and uncoupled nitric oxide synthase are major sources of glomerular superoxide in rats with experimental diabetic nephropathy. *Am J Physiol Renal Physiol* 288: F1144–F1152, 2005.
25. Shimokawa H, Yasutake H, Fujii K, Owada MK, Nakaike R, Fukumoto Y, Takayanagi T, Nagao T, Egashira K, Fujishima M, and Takeshita A. The importance of the hyperpolarizing mechanism increases as the vessel size decreases in endothelium-dependent relaxations in rat mesenteric circulations. *J Cardiovasc Pharmacol* 28: 703–711, 1996.
26. Shimokawa H. Primary endothelial dysfunction: atherosclerosis. *J Mol Cell Cardiol* 31: 23–37, 1999.
27. Siegel G, Emden J, Wenzel K, Mironneau J, and Stock G. Potassium channel activation in vascular smooth muscle. *Adv Exp Med Biol* 311: 53–72, 1992.
28. Steenbergen C, Murphy E, Levy L, and London RE. Elevation in cytosolic free calcium concentration early in myocardial ischemia in perfused rat heart. *Circ Res* 60: 700–707, 1987.
29. Taylor HJ, Chaytor AT, Evance WH, and Griffith TM. Inhibition of the gap junctional component of endothelium-dependent relaxations in rabbit iliac artery by 18-alpha glycyrrhetinic acid. *Br J Pharmacol* 125: 1–3, 1998.
30. Tiefenbacher CP, Chilian WM, Mitchell M, and Defily DV. Restoration of endothelium-dependent vasodilation after reperfusion injury by tetrahydrobiopterin. *Circulation* 94: 1423–1429, 1996.
31. Traverse JH, Chen Y, Crampton M, Voss S, and Bache RJ. Increased extravascular forces limit endothelium-dependent and -independent coronary vasodilation in congestive heart failure. *Cardiovasc Res* 52: 454–461, 2001.
32. Yada T, Hiramatsu O, Kimura A, Goto M, Ogasawara Y, Tsujioka K, Yamamori S, Ohno K, Hosaka H, and Kajiya F. In vivo observation of subendocardial microvessels of the beating porcine heart using a needle-probe videomicroscope with a CCD camera. *Circ Res* 72: 939–946, 1993.
33. Yada T, Hiramatsu O, Kimura A, Tachibana H, Chiba Y, Lu S, Goto M, Ogasawara Y, Tsujioka K, and Kajiya F. Direct in vivo observation of subendocardial arteriolar responses during reactive hyperemia. *Circ Res* 77: 622–631, 1995.
34. Yada T, Goto M, Hiramatsu O, Tachibana H, Toyota E, Nakamoto H, Ogasawara Y, Matsuda H, Arakawa K, Hayashi K, Suzuki H, and Kajiya F. In vivo visualization of subendocardial arteriolar response in renovascular hypertensive hearts. *Am J Physiol Heart Circ Physiol* 284: H1785–H1792, 2003.
35. Yada T, Shimokawa H, Hiramatsu O, Kajita T, Shigeto F, Goto M, Ogasawara Y, and Kajiya F. Hydrogen peroxide, an endogenous endothelium-derived hyperpolarizing factor, plays an important role in coronary autoregulation in vivo. *Circulation* 107: 1040–1045, 2003.
36. Yada T, Shimokawa H, Hiramatsu O, Kajita T, Shigeto F, Tanaka E, Shinozaki Y, Mori H, Kiyooka T, Katsura M, Ohkuma S, Goto M, Ogasawara Y, and Kajiya F. Beneficial effect of hydroxyfasudil, a specific Rho-kinase inhibitor, on ischemia-reperfusion injury in canine coronary microcirculation in vivo. *J Am Coll Cardiol* 45: 599–607, 2005.
37. Yaguchi Y, Satoh H, Wakahara N, Katoh H, Uehara A, Terada H, Fujise Y, and Hayashi H. Protective effects of hydrogen peroxide against ischemia/reperfusion injury in perfused rat hearts. *Circ J* 67: 253–258, 2003.

European Heart Journal (2006) 27, 1159–1165
doi:10.1093/eurheartj/ehi876

Intensive treatment of risk factors in patients with type-2 diabetes mellitus is associated with improvement of endothelial function coupled with a reduction in the levels of plasma asymmetric dimethylarginine and endogenous inhibitor of nitric oxide synthase

Satoshi Yasuda*†, Shunichi Miyazaki, Munetake Kanda, Yoichi Goto, Masaaki Suzuki, Yutaka Harano, and Hiroshi Nonogi

Division of Cardiology, Department of Medicine, National Cardiovascular Center, 5-7-1 Fujishiro-dai, Suita, Osaka 565-8565, Japan

Received 11 July 2004; revised 20 February 2006; accepted 23 March 2006; online publish-ahead-of-print 20 April 2006

KEYWORDS
Diabetes mellitus;
Endothelium;
Glucose;
Growth substances;
Nitric oxide

Aims Vascular endothelium is a major organ involved in hyperglycaemia and is affected by plasma asymmetric dimethylarginine (ADMA). ADMA is an endogenous, competitive inhibitor of nitric oxide synthase and is induced by inflammatory cytokines of tumour necrosis factor (TNF)-α *in vitro*. We hypothesized that a tight glycaemic control may restore endothelial function in patients with type-2 diabetes mellitus (DM), in association with modulation of TNF-α and/or reduction of ADMA level.

Methods and results In 24 patients with type-2 DM, the flow-mediated, endothelium-dependent dilation (FMD: %) of brachial arteries during reactive hyperaemia was determined by a high-resolution ultrasound method. Blood samples for glucose, cholesterol, TNF-α, and ADMA analyses were also collected from these patients after fasting. No significant glycaemic or FMD changes were observed in 10 patients receiving the conventional therapy. In 14 patients who were hospitalized and intensively treated, there was a significant decrease in glucose level after the treatment [from 190 ± 55 to 117 ± 21 (mean ± SD) mg/dL, $P < 0.01$]. After the intensive control of glucose level, FMD increased significantly (from 2.5 ± 0.9 to 7.2 ± 3.0%), accompanied by a significant ($P < 0.01$) decrease in TNF-α (from 29 ± 16 to 11 ± 9 pg/dL) and ADMA (from 4.8 ± 1.5 to 3.5 ± 1.1 μM/L) levels. The changes in FMD after treatment correlated inversely with those in TNF-α ($R = -0.711$, $P < 0.01$) and ADMA ($R = -0.717$, $P < 0.01$) levels.

Conclusion The intensive correction of hyperglycaemia is associated with the improvement of endothelial function, which is coupled with the decrease in the levels of reduction of plasma TNF-α and ADMA in patients with type-2 DM. A strict glycaemic control may exert anti-cytokine and anti-atherogenic effects and may therefore be pathophysiologically important.

Introduction

Cardiovascular disease is the major cause of morbidity and mortality in patients with type-2 diabetes mellitus (DM),[1] in whom hyperglycaemia is one of the main metabolic abnormalities.[2] Blood glucose control occupies the centre stage in DM management.[3] A recent controlled trial, i.e. the United Kingdom Prospective Diabetes Study (UKPDS), suggested that an intensive glucose-lowering treatment decreases the occurrence of macrovascular complications.[4] However, the exact roles of hyperglycaemia and glycaemic control in cardiovascular complications remain to be determined in patients with type-2 DM.

Previous studies demonstrated that acute hyperglycaemia impairs endothelium-dependent vasodilation in healthy subjects[5,6] and further depresses it in patients with type-2 DM.[6] These findings indicate a possible link between glucose level and endothelial function in humans. Endothelial dysfunction is an important phenomenon in the pathogenesis of atherosclerosis[7] and is related to the derangements of nitric oxide (NO) synthase in the vessel wall.[8] Asymmetric dimethylarginine (ADMA) is an endogenous, competitive inhibitor of NO synthase.[9] Its concentration is increased by tumour necrosis

* Corresponding author. Tel: +81 22 717 7153; fax: +81 22 717 7156.
E-mail address: syasuda@cardio.med.tohoku.ac.jp
† Present address: Department of Cardiovascular Medicine, Tohoku University Graduate School of Medicine, 1-1 Seiryomachi, Aobaku, Sendai 980-8574, Japan.

factor-α (TNF-α),[10] which is implicated as an important factor in the pathogenesis of type-2 DM.[11]

Thus, the present study was designed to investigate whether an intensive therapy of hyperglycaemia may improve endothelial function in association with the modulation of the cytokines and/or decrease in plasma ADMA level in patients with type-2 DM.

Methods

Study patients

The study protocol was approved by the Institutional Review board, and all these patients gave their written informed consent to participate in the study. Type-2 DM was defined according to the criteria of the Diagnosis and Classification of Diabetes Mellitus.[12] Between May 1999 and June 2000, type-2 DM patients with poor glycaemic control [fasting blood glucose >200 mg/dL and/or haemoglobin A-1C (Hb A-1C) >9%] were recruited for intensive treatment of hyperglycaemia during hospitalization. Twenty-four patients were initially assessed for inclusion in the study. Among them, 14 patients [nine men and five women, mean age 61 ± 12 (SD) years] gave their consent and were admitted to the Hospital of the National Cardiovascular Center (intensive treatment group). The remaining 10 patients [seven men and three women, mean age 63 ± 15 (SD) years], who refused to be hospitalized and were obliged to keep conventional (non-intensive) diabetes treatment, served as the control group in the present study.

All the patients underwent history screening, physical examination, and laboratory analysis, including a complete blood count: the levels of plasma electrolyte, glucose, insulin, Hb A-1C, blood urea nitrogen, creatinine, transaminases and urinary protein levels, and lipid profile. Moreover, the patients were assessed for the presence of diabetic complication, i.e. retinopathy, neuropathy, nephropathy, a history of myocardial infarction, and the presence of angina pectoris and arteriosclerosis obliterans. Patients with nephrotic-range proteinuria, thyroid disease, apparent infections, or haematologic, hepatic, or renal disease were excluded from the study. Before admission, five patients had been receiving angiotensin-converting enzyme inhibitors for hypertension and five patients receiving statin for hyperlipidaemia for over 6 months. These medications were not changed throughout the study period. In addition, no new drugs other than insulin or oral hypoglycaemic agents were administered to any of these patients.

Study design

On admission, following an overnight fasting, a non-invasive assessment of brachial arterial vasoreactivity in response to reactive hyperaemia or nitroglycerin was performed with blood sampling for the determination of the levels of glucose, insulin, Hb A-1C, total cholesterol, triglyceride, HDL cholesterol, LDL cholesterol, TNF-α, and ADMA in the plasma. We also measured plasma hepatocyte growth factor (HGF) level. The HGF may protect against endothelial dysfunction, and its production is suppressed by high glucose levels.[13] Body mass index (BMI) was calculated using the formula BMI = weight (kg)/height^2 (m^2). All measurements were repeated after ~1 month of intensive treatment for hyperglycaemia.

The intensive therapy was aimed at maintaining normal fasting glucose (80–115 mg/dL) and pre-prandial blood glucose (<130 mg/dL) levels. Throughout the study, the patients followed a 1200–1300 Kcal diet regimen of 60–65 g of protein, 30–35 g of fat, and 160–170 g of carbohydrates. The level of dietary cholesterol was 350 g/day. The dose of oral anti-diabetic drugs was adjusted accordingly and/or insulin therapy was administered to improve glycaemic control. The patients were examined once or twice a week over a 4–5-week period of blood glucose monitoring. None of the patients experienced a hypoglycaemic reaction during the study.

Brachial artery ultrasound

Flow-mediated, endothelium-dependent vasodilation (FMD) following reactive hyperaemia and endothelium-independent nitroglycerin-induced vasodilation of the brachial artery were assessed using a high-resolution ultrasound machine (System Five, General Electronics) equipped with a 7.5 MHz linear array transducer.[6] After a 10 min rest in a temperature-controlled room (22–23°C), the diameter of the right brachial artery and baseline forearm flow velocity were measured. Increased forearm blood flow was induced by the inflation of a blood pressure cuff placed around the forearm to 200 mmHg or to a pressure of 50 mmHg greater than the systolic blood pressure. This was followed by deflation (RD2 Cuff Deflator, Hokanson Inc., Bellevue, WA, USA) after 5 min. Repeated blood flow scans were obtained to measure the diameter of the brachial artery. After 15 min of vessel recuperation, a repeated measurement of the diameter of the resting brachial artery and repeated blood flow scans were obtained. Sublingual nitroglycerin (0.4 mg) was administered, and then final scans were obtained after 3 min. Throughout the study, a single lead electrocardiogram was obtained, and blood pressure was measured in the left arm every 2 min by an automated blood pressure recorder.

Ultrasound images were recorded on an S-VHS videocassette recorder. Depth and gain settings were used to optimize the images of the lumen–arterial wall interface. Vessel diameter was measured in triplicate at end diastole, from the anterior to the posterior interface between the media and the adventitia. Flow-mediated vasodilation was calculated as the ratio of brachial artery diameter after reactive hyperaemia to baseline diameter and expressed as a per cent increase. Nitroglycerin-mediated vasodilation was calculated in an analogous manner. Volumetric flow rate was calculated by multiplying the time velocity integral of the angle (~70°)-corrected Doppler flow signal by the heart rate and the vessel cross-sectional area. Changes in blood flow were expressed as the percentages of the resting flow measurements. All measurements were performed with the observers blind to patient information and study date. Using this methodology and analysis, the intra- and inter-observer variabilities in brachial artery diameter were 0.03 ± 0.02 (mean ± SD) and 0.06 ± 0.02 mm, respectively, and the variability in FMD performed on two different days was 1.4 ± 0.5%.

Laboratory measurements

Fasting plasma glucose level was measured by the glucose oxidase method and Hb A-1C level was measured by automated high-performance liquid chromatography. Insulin level was measured by the conventional radioimmunoassay. To assess insulin resistance, we used the following homeostasis model assessment (HOMA) parameters: HOMA-R = [fasting blood glucose (mg/dL) × fasting insulin (μU/mL)]/405.[14]

Total cholesterol, triglyceride, and HDL cholesterol levels were determined as described previously.[15] LDL cholesterol level was calculated using the Friedewald equation.[16]

TNF-α and HGF levels were determined by enzyme-linked immunosorbent assay (Otsuka Pharmaceutical Co., Tokushima, Japan). The detection limits of these methods are 2 pg/mL for TNF-α and 0.1 ng/mL for HGF. The intra- and inter-assay coefficients of variation were both ~7% for the enzyme-linked immunosorbent assay.

Plasma ADMA concentration was measured using high-performance liquid chromatography with pre-column derivatization, as previously described.[17] In brief, equilibrated CBA columns

Table 1 Patient characteristics

	Standard therapy (control), $n = 10$	Intensive therapy, $n = 14$	P-value
Age (years), mean ± SD	63 ± 15	61 ± 12	0.7201
Male, *n* (%)	7 (70%)	9 (64%)	0.7697
Risk factors			
Hypertension, *n* (%)	5 (50%)	7 (50%)	1.000
Hyperlipidaemia, *n* (%)	6 (60%)	7 (50%)	0.9448
Smoking, *n* (%)	4 (40%)	5 (36%)	0.8307
Retinopathy, *n* (%)	2 (20%)	2 (14%)	0.7111
Proteinuria, *n* (%)	2 (20%)	4 (29%)	0.6326
CAD, *n* (%)	2 (20%)	3 (21%)	0.9323
Peripheral artery disease, *n* (%)	0 (0%)	2 (14%)	0.6175
Stroke, n (%)	1 (10%)	1 (7%)	0.8028
Medications, baseline[a]			
ACE-inhibitor, *n* (%)	4 (40%)	5 (36%)	0.8307
Calcium blocker, *n* (%)	2 (20%)	1 (7%)	0.7543
Beta-blocker, *n* (%)	2 (20%)	1 (7%)	0.7543
Statin, *n* (%)	6 (60%)	5 (36%)	0.4462
Sulphonylurea, *n* (%)	7 (70%)	10 (71%)	0.9395
Biguanide, *n* (%)	1 (10%)	1 (7%)	0.7543
α-Glucosidase inhibitor, *n* (%)	4 (40%)	2 (14%)	0.3380

ACE, angiotensin-converting enzyme.
[a]Medications immediately before additional therapy for dysglycaemia.

(Bond Elut, Varian Inc., CA, USA) were used for three-fold washing with 1 mL serum samples with methanol and distilled water. Thereafter, the samples were eluted with 10% ammonia and dried. The sediment obtained was dissolved in 1 mL of water, the solution was centrifuged, and the supernatant was subjected to high-performance liquid chromatography using ODS columns (Fisher Scientific, St Louis, MO, USA). ADMA concentration was calculated on the basis of the recovery rate of L-monomethyl-arginine (Sigma, St Louis, MO, USA), used as the internal standard. Intra- and inter-assay variabilities were both ~6%, with a detection limit of 0.1 μM/L.

Statistical analyses

Sample size calculations were performed using a primary endpoint variable of FMD. Power calculations indicated that to detect a mean difference in FMD of 4% (SD, 3%), 13 subjects would be needed to complete the study (α statistics, 0.05; power >0.9). All data are expressed as mean ± SD. Two-tailed *t*-tests or the Mann–Whitney *U* test was used to compare the changes in response to treatment. To compare the proportions of patients, Fisher's exact test was used. Linear regression curves and correlations were calculated according to the least-squares method. *P*-values less than 0.05 were considered significant.

Results

The baseline characteristics of 10 control patients who received standard therapy and 14 intensively treated patients are summarized in *Table 1*. All 24 patients completed 3–4-week follow-up measurements.

The control patients were treated by diet alone (three patients) or diet plus oral hypoglycaemic agents (an increased dose of sulphonylurea, six patients and addition of metformin to sulphonylurea, one patient). *Table 2* shows no significant improvements in clinical and biochemical parameters during the observation period of 28 ± 5 days of standard therapy. Neither the fasting blood glucose (from 181 ± 42 to 186 ± 38 mg/dL) nor the response of FMD to reactive hyperaemia (from 3.0 ± 1.3 to 2.6 ± 1.0%) changed.

Table 2 Changes in biochemical and clinical parameters before and after standard treatment of hyperglycaemia in 10 control patients with type-2 DM

	Before	After	P-value
Hb A-1C (%)	9.4 ± 2.2	9.4 ± 2.0	>0.999
Insulin (μU/mL)	4.2 ± 2.0	4.4 ± 2.2	0.834
HOMA-R	1.9 ± 1.2	1.8 ± 1.0	0.842
Total cholesterol (mg/dL)	212 ± 28	210 ± 25	0.868
TG (mg/dL)	128 ± 40	129 ± 45	0.959
HDL cholesterol (mg/dL)	50 ± 19	51 ± 20	0.910
LDL cholesterol (mg/dL)	128 ± 22	127 ± 25	0.925
Systolic BP (mmHg)	139 ± 18	138 ± 20	0.908
Diastolic BP (mmHg)	76 ± 8	78 ± 10	0.627
BMI (kg/m^2)	23.8 ± 2.7	23.4 ± 3.1	0.763

TG, triglyceride; BP, blood pressure. Values are expressed as mean ± SD.

Biochemical and clinical changes after intensive treatment of hyperglycaemia

In the intensive therapy group, the patients were all treated by diet alone (three patients), diet plus oral hypoglycaemic agents (sulphonylurea newly given, one patient; an increased dose of sulphonylurea, one patient; addition of metformin to sulphonylurea, two patients; and addition of α-glucosidase inhibitor to sulphonylurea, one patient), or diet plus insulin (switched from oral hypoglycaemic agents, six patients). The duration of intensive treatment of hyperglycaemia was 34 ± 13 days. Clinical and biochemical parameters at baseline (before treatment) were similar between the standard therapy group and the intensive therapy group (*Tables 2* and *3*). After the intensive

Table 3 Changes in biochemical and clinical parameters before and after intensive treatment of hyperglycaemia in 14 patients with type-2 DM

	Before	After	*P*-value	*P*-value (vs. control after)
Hb A-1C (%)	9.7 ± 1.6	8.6 ± 1.4	0.032	0.287
Insulin (μU/mL)	4.4 ± 2.6	5.3 ± 2.0	0.314	0.233
HOMA-R	2.0 ± 1.1	1.6 ± 0.5	0.226	0.524
Total cholesterol (mg/dL)	202 ± 33	173 ± 28	0.019	0.003
TG (mg/dL)	121 ± 43	105 ± 51	0.378	0.246
HDL cholesterol (mg/dL)	52 ± 21	52 ± 17	>0.999	0.896
LDL cholesterol (mg/dL)	125 ± 25	101 ± 29	0.027	0.032
Systolic BP (mmHg)	134 ± 18	128 ± 14	0.779	0.1626
Diastolic BP (mmHg)	77 ± 7	74 ± 8	0.301	0.2880
BMI (kg/m^2)	23.6 ± 3.6	21.4 ± 3.2	0.049	0.1405

Values are expressed as mean ± SD.

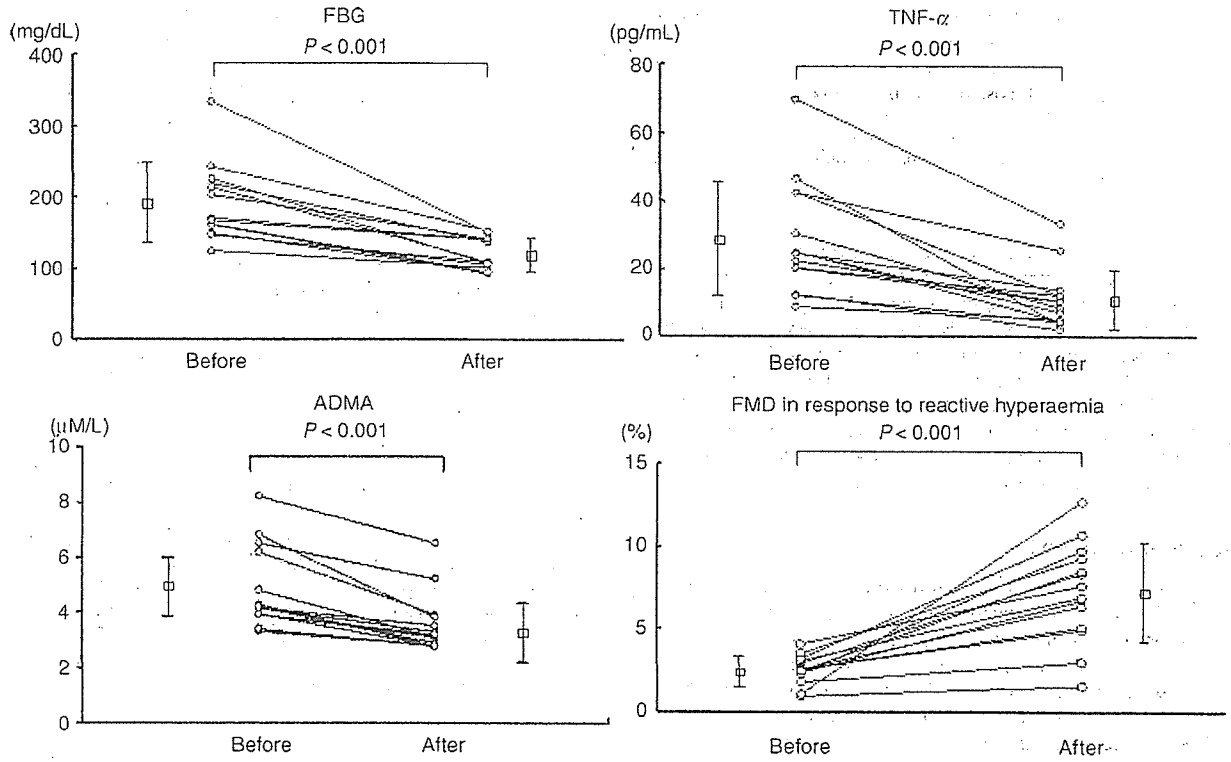

Figure 1 Individual measurements of fasting blood glucose (FBG), TNF-α and ADMA levels, and FMD in response to reactive hyperaemia before and after intensive treatment of hyperglycaemia in 14 patients with type-2 DM.

treatment, the fasting glucose level significantly decreased from 190 ± 55 to 117 ± 21 mg/dL ($P < 0.001$), as shown in *Figure 1*. Significant decreases in Hb A-1C, total cholesterol, and LDL cholesterol levels and BMI were observed, whereas no changes in HOMA-R index; insulin, triglyceride, or HDL cholesterol levels; and systolic and diastolic blood pressures were observed (*Table 3*). Two of three patients with coronary artery disease were taking statins at the time of the study.

The levels of plasma TNF-α (from 29 ± 16 to 11 ± 9 pg/dL, $P < 0.001$) and ADMA (from 4.8 ± 1.5 to 3.5 ± 1.1 μM/L, $P < 0.001$) significantly decreased after the intensive control of glucose level (*Figure 1*). However, HGF level did not significantly change throughout the study (from 0.19 ± 0.05 to 0.20 ± 0.08 ng/mL).

Brachial artery reactivity after intensive treatment of hyperglycaemia

Before treatment under hyperglycaemic condition, the baseline brachial arterial diameter was 4.5 ± 0.3 mm, and FMD in response to reactive hyperaemia was 2.4 ± 0.9%. After the intensive control of glucose level, FMD significantly ($P < 0.001$) increased to 7.2 ± 3.1% (*Figure 1*), whereas the baseline diameter (4.5 ± 0.2 mm) did not change. There was a similar increase in blood flow during reactive

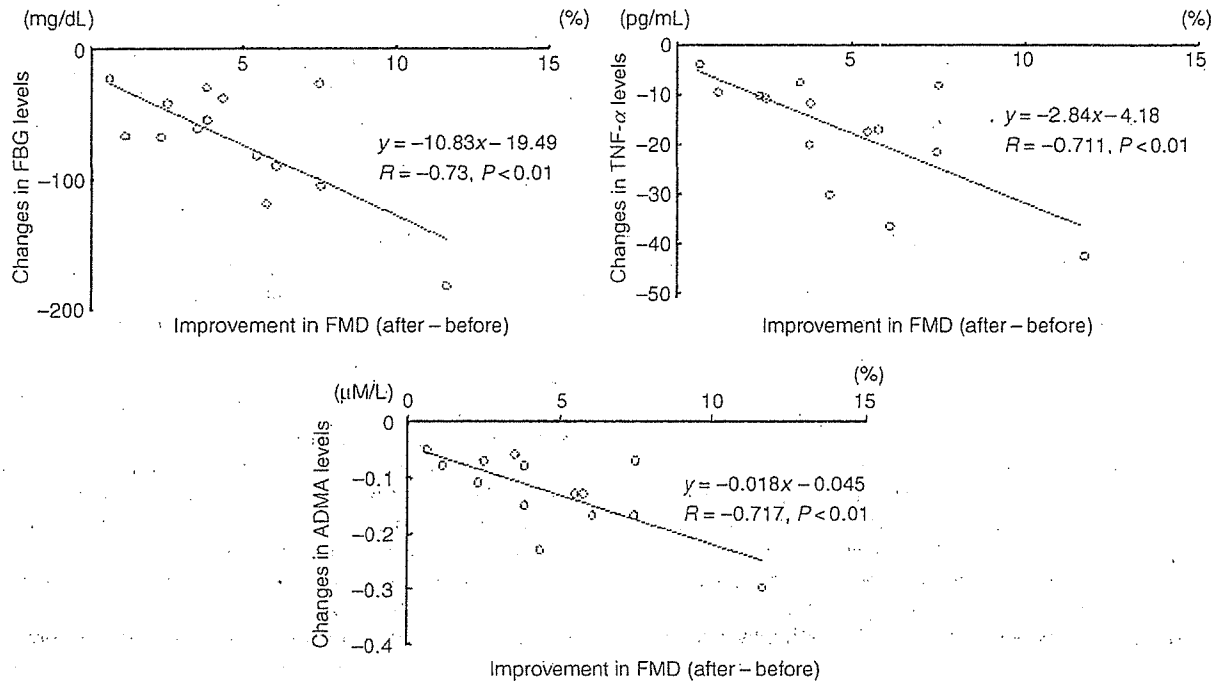

Figure 2 Correlation of improvement of FMD after treatment with decreases in levels of FBG, TNF-α, and ADMA.

hyperaemia (293 ± 16 vs. 296 ± 20%) and a similar baseline heart rate (67 ± 7 vs. 65 ± 8 bpm) before and after the treatment.

Nitroglycerin-mediated vasodilation was 9.8 ± 1.0% before treatment; however, in contrast to FMD, it did not change after treatment (10.0 ± 1.6%).

Correlation with FMD improvement

As shown in *Figure 2*, the improvement of FMD after treatment correlated inversely with the changes in fasting glucose ($R = -0.730$, $P < 0.01$), TNF-α ($R = -0.711$, $P < 0.01$), and ADMA ($R = -0.717$, $P < 0.01$) levels. However, the improvement of FMD did not correlate significantly with the changes in Hb A-1C level ($R = 0.408$, $P = 0.148$), total cholesterol level ($R = 0.325$, $P = 0.256$), or BMI ($R = 0.270$, $P = 0.351$).

Six-to-12-month follow-up

A follow-up study was performed 6–12 months after the discharge. In eight of 14 patients with an Hb A-1C level of <8.0% at this follow-up period, fasting blood glucose level and FMD remained at 127 ± 26 mg/dL and 8.4 ± 1.0%, respectively. In contrast, in the remaining six patients with an Hb A-1C level of ≥8.0%, fasting blood glucose level and FMD worsened to be 178 ± 30 mg/dL and 3.1 ± 1.1%, respectively. There were inverse correlations of FMD with fasting blood glucose ($R = -0.577$) and Hb A-1C levels ($R = -0.860$).

Discussion

The major finding in the present study is that the intensive treatment of hyperglycaemia is associated with the improvement of endothelial function, coupled with the decrease in plasma TNF-α and ADMA (an endogenous inhibitor of NO synthase) levels in patients with type-2 DM.

Previous studies revealed that an acute increase in blood glucose level impairs endothelium-dependent vasodilation in healthy subjects[5,6] and further inhibits it in patients with type-2 DM.[6] DM is a state of chronic hyperglycaemia, and glycaemic control is one of the major goals of diabetes management.[18] As shown in *Figure 1*, endothelial dysfunction improves after a 5-week intervention targeting hyperglycaemia in type-2 diabetes patients, accompanied by a relatively small but significant decrease in Hb A-1C level. In contrast, either hyperglycaemia or endothelial function did not change in control outpatients who received routine treatment. These findings suggest that hyperglycaemia may be a fundamental abnormality underlying the mechanism that causes endothelial dysfunction in DM. However, we must acknowledge a potential limitation that an appropriate control group should have included patients who were admitted to the hospital, but did not receive intensive treatment. In addition, the number of statistical tests performed and relatively small sample size of the study population may potentially infiltrate type-I error.

In patients with type-2 DM, TNF-α levels were elevated in both blood and tissue.[19–21] Taken together with results from knockout mice deficient in TNF-α or its receptors,[11] it is suggested that TNF-α is a factor contributing to the pathogenesis of type-2 DM. Hyperglycaemia is an important stimulus for TNF-α synthesis in human peripheral monocytes *in vitro*.[22] A previous *in vivo* study demonstrated that the administration of TNF-α impairs endothelial-dependent vasodilation in rats.[23] In the present study, as shown in *Figure 1*, plasma TNF-α level decreased after the intensive treatment of hyperglycaemia. This finding indicates the therapeutic potential of a strict glycaemic control against inflammatory cytokines that play a prominent role in atherogenesis.[7]

TNF-α and hyperglycaemia could impair dimethylarginine dimethylaminohydrolase and cause the accumulation of ADMA, an endogenous, competitive inhibitor of NO synthase, contributing to the derangements of NO pathways in the vessel.[10,24] The intra-arterial infusions of ADMA significantly impair endothelium-dependent flow responses in the human forearm.[25] In the present study, we found that the ADMA level increased in patients with type-2 DM (*Figure 1*), and its decrease after the strict glycaemic control correlated significantly with the improvement of FMD (*Figure 2*). Not only ADMA, but also TNF-α itself downregulates NO synthase by decreasing mRNA's half-life.[26] Moreover, both inflammatory cytokines and high glucose levels enhance the production of oxygen-derived free radicals,[27,28] which rapidly inactivate NO.[29] In patients with type-2 DM, the extent of urinary excretion of the isoprostanes (8-iso-prostaglandin $F_{2\alpha}$) significantly decreased ~4 weeks after an intensive therapy for hyperglycaemia, an intervention similar to that used in the present study.[30] Taking together a recent report that lowering serum TNF-α level alone (without glycaemic control) does not improve endothelial function,[31] these findings suggest that the hyperglycaemia-induced oxidative stress could be a key factor in the pathophysiology of diabetes.

HGF is characterized to be one of the most potent mitogens among the growth factors for vascular endothelial cells and contributes to vascular protection or repair.[13] Because its production is suppressed by glucose in a dose-dependent manner *in vitro*,[13] we hypothesized that endothelial dysfunction might be associated with the decreased production of HGF in diabetic patients. However, this was not the case. The level of HGF did not change throughout this study. Moreover, as shown in *Table 3*, insulin sensitivity, as assessed using HOMA-R index,[14] did not change significantly. Insulin resistance contributes, in part, to the pathogenesis of type-2 DM and may be potentially linked with endothelial dysfunction and ADMA.[32] To address this important issue, we need to further assess insulin sensitivity with a more specific method such as steady-state plasma glucose measurement.

Impaired endothelium is a key factor for diabetic macroangiopathy.[7] Thus, restoring endothelial function has important clinical implications for reducing the risk of cardiovascular diseases in diabetic patients. The present results, although obtained in a short period, suggest that a long-term maintenance of strict glycaemic control is important. If hyperglycaemia continues, then the expression level of NO synthase and the generation of NO may be chronically reduced, leading to a persistent dysfunction of the vascular endothelium and the consequent atherogenesis. In the UKPDS conducted for more than 15 years,[4] the difference in Hb A-1C level between the conventionally and intensively treated groups was significant throughout the study. However, Hb A-1C level progressively increased in both groups. The median Hb A-1C level was 6.6% in the first 5 years, but increased to 8.1% in the last 5 years, even in the intensively treated group. A difficulty in maintaining a good glycaemic control may explain, in part, the borderline decrease in the extent of myocardial infarction ($P = 0.05$) induced by the intensive treatment. Taking the multifactorial aetiology of macrovascular disease into account, the results of the UKPDS also suggest that the optimum treatment of patients with type-2 DM would include the control of blood pressure and correction of lipid abnormalities in addition to the control of glucose level. For the assessment of the effectiveness of therapeutic/dietary interventions and for the early detection of vascular dysfunction, plasma ADMA may be useful as a potential biochemical marker.[9,33] Metformin,[34] angiotensin-converting enzyme inhibitors/angiotensin II receptor blocker,[35] and statins[36] could decrease ADMA level. Although these drugs were not newly given in the present patients, it is possible that an increased utilization of and compliance with medications and an improved diet during hospitalization may contribute, at least in part, to endothelial function improvement. Insulin-sensitizing rosiglitazone also decreases ADMA level.[37] A recent study has suggested that obese and insulin resistance are not strongly associated with the development of type-2 DM in Japanese patients with a BMI of ~23 kg/m^2 (from the Japan Diabetes Complications Study), unlike in European patients with a BMI of ~29 kg/m^2 (from the UKPDS).[38]

In conclusion, in patients with type-2 DM, the intensive treatment of hyperglycaemia is associated with the improvement of endothelial dysfunction, coupled with decreases in TNF-α and ADMA levels. A strict glycaemic control may exert anti-cytokine and anti-atherogenic effects and may therefore be pathophysiologically important.

Acknowledgement

This study was supported partly by a grant for Clinical Vascular Function from Kimura Memorial Foundation (Fukuoka, Japan) and by the Promotion of Fundamental Studies in Health Science of the Organization for Pharmaceutical Safety and Research of Japan (Tokyo, Japan).

Conflict of interest: none declared.

References

1. Haffner SM, Lehto S, Ronnemaa T, Pyorala K, Laakso M. Mortality from coronary heart disease in subjects with type 2 diabetes and in nondiabetic subjects with and without prior myocardial infarction. *N Engl J Med* 1998;339:229–234.
2. Capes SE, Hunt D, Malmberg K, Gerstein HC. Stress hyperglycaemia and increased risk of death after myocardial infarction in patients with and without diabetes: a systematic overview. *Lancet* 2000;355:773–778.
3. Grundy SM, Benjamin IJ, Burke GL, Chait A, Eckel RH, Howard BV, Mitch W, Smith SC Jr, Sowers JR. Diabetes and cardiovascular disease: a statement for healthcare professionals from the American Heart Association. *Circulation* 1999;100:1134–1146.
4. UK Prospective Diabetes Study (UKPDS) Group. Intensive blood-glucose control with sulphonylureas or insulin compared with conventional treatment and risk of complications in patients with type 2 diabetes (UKPDS 33). *Lancet* 1998;352:837–853.
5. Williams SB, Goldfine AB, Timimi FK, Ting HH, Roddy MA, Simonson DC, Creager MA. Acute hyperglycemia attenuates endothelium-dependent vasodilation in humans *in vivo*. *Circulation* 1998;97:1695–1701.
6. Kawano H, Motoyama T, Hirashima O, Hirai N, Miyao Y, Sakamoto T, Kugiyama K, Ogawa H, Yasue H. Hyperglycemia rapidly suppresses flow-mediated endothelium-dependent vasodilation of brachial artery. *J Am Coll Cardiol* 1999;34:146–154.
7. Ross R. Atherosclerosis—an inflammatory disease. *N Engl J Med* 1999; 340:115–126.
8. Harrison DG. Cellular and molecular mechanisms of endothelial cell dysfunction. *J Clin Invest* 1997;100:2153–2157.
9. Cooke JP. Does ADMA cause endothelial dysfunction? *Arterioscler Thromb Vasc Biol* 2000;20:2032–2037.

10. Ito A, Tsao PS, Adimoolam S, Kimoto M, Ogawa T, Cooke JP. Novel mechanism for endothelial dysfunction: dysregulation of dimethylarginine dimethylaminohydrolase. *Circulation* 1999;99:3092-3095.
11. Moller DE. Potential role of TNF-alpha in the pathogenesis of insulin resistance and type 2 diabetes. *Trends Endocrinol Metab* 2000;11: 212-217.
12. The Expert Committee on the Diagnosis and Classification of Diabetes Mellitus. Report of the expert committee on the diagnosis and classification of diabetes mellitus. *Diabetes Care* 1997;20:1183-1197.
13. Morishita R, Nakamura S, Nakamura Y, Aoki M, Moriguchi A, Kida I, Yo Y, Matsumoto K, Nakamura T, Higaki J, Ogihara T. Potential role of an endothelium-specific growth factor, hepatocyte growth factor, on endothelial damage in diabetes. *Diabetes* 1997;46:138-142.
14. Matthews DR, Hosker JP, Rudenski AS, Naylor BA, Treacher DF, Turner RC. Homeostasis model assessment: insulin resistance and beta-cell function from fasting plasma glucose and insulin concentrations in man. *Diabetologia* 1985;28:412-419.
15. Shinozaki K, Suzuki M, Ikebuchi M, Takaki H, Hara Y, Tsushima M, Harano Y. Insulin resistance associated with compensatory hyperinsulinemia as an independent risk factor for vasospastic angina. *Circulation* 1995;92:1749-1757.
16. Friedewald WT, Levy RI, Fredrickson DS. Estimation of the concentration of low-density lipoprotein cholesterol in plasma, without use of the preparative ultracentrifuge. *Clin Chem* 1972;18:499-502.
17. Pettersson A, Uggla L, Backman V. Determination of dimethylated arginines in human plasma by high-performance liquid chromatography. *J Chromatogr B Biomed Sci Appl* 1997;692:257-262.
18. Keen H, Clark C, Laakso M. Reducing the burden of diabetes: managing cardiovascular disease. *Diabetes Metab Res Rev* 1999;15:186-196.
19. Winkler G, Salamon F, Harmos G, Salamon D, Speer G, Szekeres O, Hajos P, Kovacs M, Simon K, Cseh K. Elevated serum tumor necrosis factor-alpha concentrations and bioactivity in type 2 diabetics and patients with android type obesity. *Diabetes Res Clin Pract* 1998;42(Suppl.):169-174.
20. Zinman B, Hanley AJ, Harris SB, Kwan J, Fantus IG. Circulating tumor necrosis factor-alpha concentrations in a native Canadian population with high rates of type 2 diabetes mellitus. *J Clin Endocrinol Metab* 1999;84:272-278.
21. Clausell N, Kalil P, Biolo A, Molossi S, Azevedo M. Increased expression of tumor necrosis factor-alpha in diabetic macrovasculopathy. *Cardiovasc Pathol* 1999;8:145-151.
22. Morohoshi M, Fujisawa K, Uchimura I, Numano F. Glucose-dependent interleukin 6 and tumor necrosis factor production by human peripheral blood monocytes *in vitro*. *Diabetes* 1996;45:954-959.
23. Wang P, Ba ZF, Chaudry IH. Administration of tumor necrosis factor-alpha *in vivo* depresses endothelium-dependent relaxation. *Am J Physiol* 1994;266:H2535-H2541.
24. Lin KY, Ito A, Asagami T, Tsao PS, Adimoolam S, Kimoto M, Tsuji H, Reaven GM, Cooke JP. Impaired nitric oxide synthase pathway in diabetes mellitus: role of asymmetric dimethylarginine and dimethylarginine dimethylaminohydrolase. *Circulation* 2002;106:987-992.
25. Calver A, Collier J, Leone A, Moncada S, Vallance P. Effect of local intra-arterial asymmetric dimethylarginine (ADMA) on the forearm arteriolar bed of healthy volunteers. *J Hum Hypertens* 1993;7:193-194.
26. Yoshizumi M, Perrella MA, Burnett JC Jr, Lee ME. Tumor necrosis factor downregulates an endothelial nitric oxide synthase mRNA by shortening its half-life. *Circ Res* 1993;73:205-209.
27. Matsubara T, Ziff M. Increased superoxide anion release from human endothelial cells in response to cytokines. *J Immunol* 1986;137: 3295-3298.
28. Marfella R, Quagliaro L, Nappo F, Ceriello A, Giugliano D. Acute hyperglycemia induces an oxidative stress in healthy subjects. *J Clin Invest* 2001;108:635-636.
29. Gryglewski RJ, Palmer RM, Moncada S. Superoxide anion is involved in the breakdown of endothelium-derived vascular relaxing factor. *Nature* 1986;320:454-456.
30. Davi G, Ciabattoni G, Consoli A, Mezzetti A, Falco A, Santarone S, Pennese E, Vitacolonna E, Bucciarelli T, Costantini F, Capani F, Patrono C. *In vivo* formation of 8-iso-prostaglandin f2alpha and platelet activation in diabetes mellitus: effects of improved metabolic control and vitamin E supplementation. *Circulation* 1999;99:224-229.
31. Bilsborough W, O'Driscoll G, Stanton K, Weerasooriya R, Dembo L, Taylor R, Green D. Effect of lowering tumour necrosis factor-alpha on vascular endothelial function in type II diabetes. *Clin Sci* 2002;103:163-169.
32. Nash DT. Insulin resistance, ADMA levels, and cardiovascular disease. *JAMA* 2002;287:1451-1452.
33. Fard A, Tuck CH, Donis JA, Sciacca R, Di Tullio MR, Wu HD, Bryant TA, Chen NT, Torres-Tamayo M, Ramasamy R, Berglund L, Ginsberg HN, Homma S, Cannon PJ. Acute elevations of plasma asymmetric dimethylarginine and impaired endothelial function in response to a high-fat meal in patients with type 2 diabetes. *Arterioscler Thromb Vasc Biol* 2000;20:2039-2044.
34. Asagami T, Abbasi F, Stuelinger M, Lamendola C, McLaughlin T, Cooke JP, Reaven GM, Tsao PS. Metformin treatment lowers asymmetric dimethylarginine concentrations in patients with type 2 diabetes. *Metabolism* 2002;51:843-846.
35. Delles C, Schneider MP, John S, Gekle M, Schmieder RE. Angiotensin converting enzyme inhibition and angiotensin II AT1-receptor blockade reduce the levels of asymmetrical N(G), N(G)-dimethylarginine in human essential hypertension. *Am J Hypertens* 2002;15:590-593.
36. Lu TM, Ding YA, Leu HB, Yin WH, Sheu WH, Chu KM. Effect of rosuvastatin on plasma levels of asymmetric dimethylarginine in patients with hypercholesterolemia. *Am J Cardiol* 2004;94:157-161.
37. Stuhlinger MC, Abbasi F, Chu JW, Lamendola C, McLaughlin TL, Cooke JP, Reaven GM, Tsao PS. Relationship between insulin resistance and an endogenous nitric oxide synthase inhibitor. *JAMA* 2002;287:1420-1426.
38. Sone H, Ito H, Ohashi Y, Akanuma Y, Yamada N; Japan Diabetes Complication Study Group. Obesity and type 2 diabetes in Japanese patients. *Lancet* 2003;361:85.

<班研究紹介シリーズ>

脳卒中に対する再生医療的技術を用いた治療法の開発に関する研究

田口　明彦[1)]　明神　和紀[1)]　松山　知弘[2)]

循環器病研究委託事業（16公-7）
「脳卒中，脳血管性痴呆症に対する再生医療技術を用いた治療法の開発に関する研究」班

<研究組織>
代表研究者
田口　明彦　国立循環器病センター
分担研究者

出澤　真理	京都大学医科学研究科	西村　浩美	先端医療振興財団
松山　知弘	兵庫医科大学医学部	林　拓也	国立循環器病センター
飯田　秀博	国立循環器病センター	植田　初江	国立循環器病センター

Key words：脳梗塞，再生医療
（脳卒中 28：433—436，2006）

緒　言

現在わが国においては，他の諸国においては類を見ないほどの急速な高齢化社会を迎えており，脳梗塞後遺症や血管性痴呆症に起因する要介護者の急激な増加は，日本の社会構造を根底から揺るがす極めて深刻な社会問題となっている．これらの疾患に対し様々な研究が積み重ねられてきたが，脳梗塞に対する確立された治療法は発症後数時間以内の血栓溶解療法以外になく，脳血管性痴呆に対しては全く有効な治療手段がないのが現状である．

近年，今までの医療では治療できなかった難治性の虚血性循環器疾患に対して，再生医療的手法を用いた治療法が開始され，虚血性心疾患や末梢動脈閉塞症に対しては著しい治療効果が報告されている．しかし，脳障害に対する治療法はほとんど進歩が見られていないのが現状であり，基礎研究レベルにおいても，ES細胞あるいは胎児由来の神経幹細胞を用いた研究が盛んに行われてきたが，それらの単なる移植では神経細胞として脳内で生着，成熟し機能することが困難であることが明らかになりつつある．

我々は胎生期や成体における神経発生や神経再生において，神経幹細胞の分化や成熟，機能は，常に血管新生とともにプログラムされていることに着目し研究を行ってきたが，本研究班では①脳梗塞治療を目的とした，脳血管再生および神経細胞再生を含む脳組織再生，機能再生による治療法の確立に向けた研究，および②脳梗塞予防を目的とした，脳血管再生による治療法の確立に向けた研究，を行っており，本総説においてその研究経過を概説します．

A. 脳梗塞治療を目的とした，脳血管再生および神経細胞再生を含む脳組織再生，機能再生による治療法の確立に向けた研究

1. 再現性の非常に高いマウス脳梗塞モデルの作成：松山，田口

脳梗塞に対する新しい治療法の効果検定には，再現性の高い動物モデルが必要不可欠であるが，既存のげっ歯類脳梗塞動物モデルはその脳梗塞発症部位およびサイズの再現性が低く，かつ脳梗塞後の生存率に大きな問題を抱えていた．そのため，治療効果の判定には一過性脳虚血モデルが広く用いられてきたが，一過

[1)]国立循環器病センター研究所循環動態機能部
[2)]兵庫医科大学医学部先端医学研究所
（2006年9月11日受付，2006年9月16日受理）